# Controls on bedrock bedform development beneath the Uummannaq Ice Stream onset zone, West Greenland

Timothy P. Lane[a,b]*, David H. Roberts[a], Brice R. Rea[c], Colm Ó Cofaigh[a], Andreas Vieli[d]

[a] Department of Geography, South Road, Durham University, UK

[b] Department of Geography, Liverpool John Moores University, Byrom Street, Liverpool L3 3AF, UK.

[c] Geography and Environment, School of Geosciences, University of Aberdeen, Meston Building, Old Aberdeen, AB24 3UE, UK

[d] Department of Geography, University of Zurich – Irchel, Winterthurerstr. 190, CH-8057 Zurich, Switzerland

*Corresponding author Timothy Lane at Department of Geography, Liverpool John Moores University, Byrom Street, Liverpool L3 3AF, UK. Tel: 00447817344057; Email: t.p.lane@ljmu.ac.uk.

## Abstract

This paper investigates the controls on the formation of subglacially eroded bedrock bedforms beneath the topographically confined region upstream of the Uummannaq Ice Stream (UIS). During the last glacial cycle, palaeoglaciological conditions are believed to have been similar for all sites in the study, characterised by thick, fast-flowing ice moving over a rigid bedrock bed. Classic bedrock bedforms indicative of glacially eroded terrain were mapped, including p-forms, roches moutonnées, and whalebacks. Bedform long axes and plucked face orientations display close correlation (parallel and perpendicular) to palaeo-ice flow directions inferred from striae measurements. Across all sites, elongation ratios (length to width) varied by an order of magnitude between 0.8:1 and 8.4:1. Bedform properties (length, height, width, and long axis orientation) from four subsample areas,

form morphometrically distinct populations, despite their close proximity and hypothesised similarity in palaeoglaciological conditions.

Variations in lithology and geological structures (e.g., joint frequency; joint dip; joint orientation; bedding plane thickness; and bedding plane dip) provide lines of geological weakness, which focus the glacial erosion, in turn controlling bedform geometries. Determining the relationship(s) between bedding plane dip relative to palaeo-ice flow and bedform shape, relative length, amplitude, and wavelength has important ramifications for understanding subglacial bed roughness, cavity formation, and likely erosion style (quarrying and/or abrasion) at the ice–bed interface. This paper demonstrates a direct link between bedrock bedform geometries and geological structure and emphasises the need to understand bedrock bedform characteristics when reconstructing palaeoglaciological conditions.

*Keywords*: ice stream; glacial erosion; bedrock bedform; abrasion; quarrying; Greenland ice sheet

## 1. Introduction

### *1.1. Importance of glacial bedforms*

An understanding of past ice sheet dynamics can significantly improve our understanding of current and potential future changes to ice sheet mass balance in Greenland and Antarctica under predicted climate-forcing scenarios. Ice streams are the most dynamic part of ice sheets, and they exert a strong influence upon mass balance (MacAyeal, 1993; Ó Cofaigh et al., 2003; Sejrup et al., 2003; Stokes et al., 2005). Bed conditions are a key control upon the functioning of ice streams and thereby the mass balance and health of the entire ice sheet. In recent years bedform analyses have been pivotal in allowing us to understand the basal conditions operating beneath ice streams onshore (Stokes and Clark, 1999; 2001; Roberts and Long, 2005; Bradwell et al., 2008; Stokes et al., 2009; Phillips et al., 2010) and offshore (Canals et al., 2002; Ó Cofaigh et al., 2002; Sejrup et al., 2003; Evans et al., 2009; Hogan et al., 2010; 2013). Ice stream onset to trunk zone transitions are recognised as being characterised by a transition in bedform type and characteristics relating to the balance between erosion and deposition (Ó Cofaigh et al., 2002; Graham et al., 2009). Onset zones are often dominated by bedrock bedforms (Kleman et al., 2008) where, on average over glacial cycles, sediment evacuation exceeds sediment generation as erosion is widespread and ice velocities typically are increasing. Trunk regions generally are dominated by soft-beds where, over glacial cycles, sediment advection of the material eroded from the upper ice stream catchment leads to deposition (e.g., Ó Cofaigh et al., 2002; Graham et al., 2009).

Sedimentary bedforms have been successfully used to decode ice stream dynamics in palaeoglaciated regions through detailed mapping of ice flow directions, inference of basal thermal regimes, delineation of fast and slow palaeo-ice flow regions, and improvement in our understanding of contemporary subglacial processes (Clark, 1993; Stokes and Clark, 2001; Ó Cofaigh

et al., 2002; Dowdeswell et al., 2008; King et al., 2009). However, subglacial bedrock bedforms remain poorly investigated and are not fully understood because of numerous glaciological and geological complexities. A growing body of research is exploring the evolution of bedrock bedforms and the implications for understanding ice sheet and ice stream dynamics. Studies have been undertaken on submarine and on terrestrial landforms, reporting roches moutonnées and whalebacks (e.g., Gordon, 1981; Sugden et al., 1992; Roberts and Long, 2005; Roberts et al., 2010; Krabbendam and Glasser, 2011), large glacially moulded bedrock ridges often controlled by bedrock structure (Roberts et al., 2010), mega-scale crag-and-tail forms (Jansson et al., 2003; Ottesen et al., 2008), erosional mega-grooves (Bradwell et al., 2008; Roberts et al., 2010), crag and tails, and other crudely streamlined bedforms with blunt stoss and tapered lee sides (Lowe and Anderson, 2002; Ó Cofaigh et al., 2002; Ó Cofaigh et al., 2013). In central west Greenland, sedimentary bedforms are sparse, and areal scour dominates low elevation terrain (< 1000 m above sea level, asl) (Sugden, 1974; Glasser and Warren, 1990; Roberts and Long, 2005), so the majority of terrestrial glacial landforms are erosional. Glacially eroded bedforms are ubiquitous in these areas, and from this evidence palaeo-ice sheet basal conditions can be reconstructed.

This paper investigates bedrock bedform evolution within the fjords that feed the onset zone of the Uummannaq Ice Stream (UIS). Firstly, it explores the relationship between bedrock bedforms and hypothesised ice flow conditions. Secondly, it considers the influence of local geology on bedform formation, and finally it considers our broader understanding of subglacial bedrock bedform genesis and evolution under ice streams.

### *1.2. Glacial erosion and bedrock bedforms*

All features of mechanical glacial erosion are formed through either abrasion or quarrying (Boulton, 1974; Rea and Whalley, 1994), both processes indicative of warm-based ice sliding across its bed

(Rea, 2007). As defined by Rea (2007), abrasion is subglacial frictional wear at the bed as debris-charged basal ice slides across it. This is enhanced as ice encounters a bedrock bump, thereby driving particles held in the ice toward the bed, increasing abrasive potential (Boulton, 1974). Erosion is achieved either through fracture of the bedrock by large particles (> 0.01 m) or through polishing by finer (< 0.01 m) material (Hindmarsh, 1996; Glasser and Bennett, 2004). Quarrying is reliant upon the presence of lee side cavities beneath the glacier, which may be water- or air-filled. Glacier sliding focuses overburden pressure on the bed, upstream of the cavity (Iverson, 1991; Hallet, 1996). This causes crack growth and block removal, especially when basal water pressures are variable (Iverson, 1991). The magnitude of plucking is heavily reliant on local effective pressure (difference between overburden pressure and cavity water pressure), bedrock structure, and cavity dimension (Iverson, 2012). Cavity formation is favoured in areas of low overburden pressure and fluctuating subglacial water pressures, most likely in areas of thin ice (Iverson, 1991). The most commonly reported small to medium features related to glacial erosion and those which will be dealt with in this paper are roches moutonnées and whalebacks. Roches moutonnées are characterised by a smooth, often abraded, curved stoss slope and a steep lee side formed through quarrying and plucking (Lindstrom, 1988; Glasser and Bennett, 2004; Roberts and Long, 2005). Quarrying of blocks from lee sides of bedrock bumps is often facilitated by subvertical joints within the bedrock (Lindstrom, 1988; Sugden et al., 1992). Conversely, whalebacks display smooth, curved stoss and lee sides resulting from abrasion across the entire bedform. Whalebacks are hypothesised to develop when cavity formation is suppressed and when continual ice-bed coupling can be achieved, restricting opportunities for cavity formation and quarrying (Evans, 1996). Previous publications provide a full discussion of the processes that form roches moutonnées and whalebacks (Glasser and Bennett, 2004; Roberts and Long, 2005).

Bedrock structure is well known to exert a direct control on subglacial bedform development, type, and morphology (Gordon, 1981; Rea and Whalley, 1994; Roberts and Long, 2005; Dühnforth et al., 2010; Roberts et al., 2010; Krabbendam and Bradwell, 2011; Krabbendam and Glasser, 2011; Hooyer et al., 2012). Variability in bedding plane strike, dip, and thickness can have a strong impact on bedform evolution (Roberts et al., 2010). High bedrock hardness increases abrasion resistance (Krabbendam and Glasser, 2011), while joint spacing can control bedform type by facilitating or resisting quarrying (Dühnforth et al., 2010; Iverson, 2012). Joint orientation can control lee side plucking, irrespective of palaeo-ice flow direction (Gordon, 1981; Rea and Whalley, 1996; Krabbendam and Bradwell, 2011; Hooyer et al., 2012).

Often, bedrock bedforms in areas of palaeo-ice streaming have low elongation ratios (the ratio of length to width: ELRs) (< 10:1), in contrast to soft sediment bedforms (> 10:1) (Roberts and Long, 2005; Roberts et al., 2010). In order for bedforms to develop high elongation ratios, a smooth (on the length scale of the landforms) ice-bed interface is required. On bedrock beds this situation is prevented by the strength of the bedrock and lack of sediment to smooth out the bed roughness. Further complexities in bedform morphology are introduced as bedform development can occur during different phases of a single glacial advance-and-retreat cycle through changes in ice-bed coupling (Roberts and Long, 2005). This means that bedforms can be modified by multiple ice advances of varying direction, developing complex, double-plucked bedforms (Roberts and Long, 2005; Roberts et al., 2010).

## 2. Study site

### *2.1. Field sites*

The field site lies within the Uummannaq region of central west Greenland, at 71.30° to 72.00° N (Fig. 1). The region covers ~25,000 km$^2$ and is topographically constrained by two large peninsulas:

139 Svartenhuk in the north and Nuussuaq in the south (Fig. 1). Repeated glaciation throughout the
140 Quaternary has produced a series of deep, coalescent fjords that broadly run east-west (Roberts et
141 al., 2013; Lane et al., 2014). Selective linear erosion has created a high relief landscape, with
142 plateaux summits reaching up to 2000 m asl and fjords reaching 1300 m below sea level. The high-
143 level plateaux terrain fosters contemporary cold-based ice caps. The study focused on Rink-Karrat
144 and Ingia Fjords (Fig. 1). In order to compare subglacial bedforms across settings of varying
145 geological structure, two subareas were selected in both Rink-Karrat and Ingia Fjords. Within Rink-
146 Karrat Fjord, subareas KA1 and KA2 are at 200-260 m asl on the eastern flank of Karrat Island (Fig.
147 2A). They are 50 km from the present margin of Rink Isbræ and 30 km from the present margin of
148 Umiámáko Isbræ. The island is small, ~28 $km^2$, and bifurcates Rink-Karrat fjord with < 300 m deep
149 water to the north and 600-700 m deep water to the south, forming a large relief (500-600 m)
150 bedrock bump within the fjord. Based upon field observations and the differences in bedform
151 morphology, KA2 was further divided into KA2i and KA2ii. Subareas IN1 and IN2 are found at 100-
152 270 m asl, on a sloping ~15 $km^2$ peninsula that forms part of the Ingia Fjord wall, 18 km from the
153 present margin of Ingia Isbræ. The depth of Ingia Fjord is not known in this region. All subareas
154 exist in regions of low relief and elevation, in regions characterised by intense areal scour. Sediment
155 cover is sparse, evidenced only by a series of gravelly lateral moraines on Karrat Island (Lane et al.,
156 2014).
157
158 *2.2. Geology*
159 The Uummannaq region is characterised by three distinct bedrock types. An Archean basement
160 forms the deeply incised inner fjord system in the east, Palaeozoic–Mesozoic sediments underlie
161 Igdlorssuit Sund, and Palaeogene volcanics bound the west of the region (Fig. 1) (Pedersen and
162 Pulvertaft, 1992; Garde and Steenfelt, 1999; Henriksen et al., 2000). The sites investigated for this
163 study are underlain by an Archaen basement and form part of the Nûkavsak Formation in the

Archaen Rinkian belt (Kalsbeek et al., 1998). Henderson and Pulvertaft (1987a) described the Nûkavsak Formation as being composed of interlayered granular semipelite, pelitic schist, and metagreywacke, interpreted as a sequence of turbidites with little lithological variation through their vertical and horizontal extent. In the field they were seen to display multiple subvertical and subhorizontal joints with beds of variable thickness (~5-20 cm). The metagreywacke was infrequently interbedded with veins of less heavily jointed quartzite up to 50 cm thick. The occurrence of quartzite bands was most pronounced in IN1 and IN2.

### *2.3. Palaeoglaciological background*

During the Last Glacial Maximum (LGM), the Uummannaq region was dominated by the UIS, a large ice stream system (Roberts et al., 2013) that reached the edge of the continental shelf (Ó Cofaigh et al., 2013; Dowdeswell et al., 2014). During the last glaciation, outlets draining the northern sector of the Uummannaq region (Ingia, Umiámáko, and Rink Isbræ) flowed south into Igdlorssuit Sund (Fig. 1) and joined ice draining from the southern sector. These branches coalesced in Igdlorssuit Sund, which became the palaeo-UIS onset zone; and confluent trunk ice flowed west through the Uummannaq Trough to the shelf edge at the LGM. Geomorphological and geochronological data have constrained the LGM upper limit of warm-based ice to 1400-1968 m asl within 50 km of the present ice sheet margin and to > 1040 m asl in the outer fjords – close to Karrat Island (Roberts et al., 2013; Lane et al., 2014). Higher elevation areas remained exposed as nunataks or were covered by protective, cold-based ice caps (Roberts et al., 2013; Lane et al., 2014). Following the LGM, the UIS began to retreat from the shelf edge by 14.9 cal. ka BP (Ó Cofaigh et al., 2013), unzipping and retreating into individual fjords. Outlet glaciers reached their present margins after 8.7 $^{10}$Be ka in the south and 5 $^{10}$Be ka in the north. A more detailed discussion of the deglacial chronology can be found in Roberts et al. (2013) and Lane et al. (2014). At the LGM, all study locations were therefore positioned within fjords that constituted upstream branches of the palaeo-UIS. Palaeoglaciological

189 reconstructions indicate that during the LGM ice would have remained broadly topographically
190 constrained within fjords (Lane et al., 2014), with overtopping of fjord mountains up to 1400 – 1968
191 m asl.
192
193 **3. Methods**
194 Initial mapping used 1:50,000 topographic maps, 1:100,000 geological maps (Henderson and
195 Pulvertaft, 1987b), and 1:150,000 aerial photographs (~5 m resolution) (Kort and Matrikelstyrelsen).
196 This initial assessment of the broad-scale topography identified regions of areal scour containing
197 bedrock bedforms for more detailed study. These regions were then mapped onto a topographic
198 base map. Subsequently, four areas were chosen for detailed field analysis (Fig. 2) based upon their
199 accessibility and the ubiquity of bedforms within them. In each area, 40 - 50 glacial bedforms were
200 identified and mapped using previously acknowledged criteria classifying them as roches
201 moutonnées (bedrock bedforms, displaying abraded stoss slopes and middle surfaces, plucked lee
202 faces with evidence of block removal) or whalebacks (bedforms with smooth stoss slopes and lee
203 slopes, evidence for widespread abrasion, and little/no evidence of plucking from lee slopes) and
204 defined by length as macro (> 100 m), meso (100– 10 m), or micro (< 10 m) features (Glasser and
205 Warren, 1990; Glasser and Bennett, 2004; Roberts and Long, 2005). Following this, bedform
206 features were recorded (bedform long axis orientation, direction of plucked face(s), and presence
207 and direction of striae). Bedform dimensions (length, width, and height) and long axis orientation
208 were measured using a tape measure, and ELRs were subsequently calculated. Transverse
209 wavelength (transverse distance between bedform crests - TW) was measured in each area using a
210 tape measure. This was used in conjunction with the bedform length to calculate bedform density
211 (bedforms/km$^2$). Bedform density estimates and differences between subareas were validated
212 through bedform counting within known areas (1 km$^2$) using aerial photographs. Bedrock lithology
213 was characterised using published reports from the region (Henderson and Pulvertaft, 1987b;

Kalsbeek et al., 1998), and bedrock structure was characterised within each study area in the field through measurement of bedding plane thickness, strike and dip, and joint density. Data from bedding planes and joints were plotted on lower hemisphere stereographic projections (stereonets), and striae were plotted on rose diagrams.

Apparent dip ($d_a$) was calculated for each subarea (Fig. 3). The $d_a$ is a measure of bedding plane dip relative to palaeo-ice flow direction, indicated in this study by striae data. Apparent dip is routinely used to measure the inclination of geological beds when not seen perpendicular to bedding plane strike (Lisle, 2004). However, here we use it to measure the bedding plane dip experienced by palaeo-ice flow. Unless ice flow was directly parallel ($d_a$ = 0) or perpendicular ($d_a$ = true dip) to bedding plane strike, the bedding plane dip that the ice encountered ($d_a$) would be somewhere between 0° and the true dip.

Apparent dip is calculated with the following equation: $d_a = \arctan ( \tan(d_t) * \sin (S_{xs} - S_b) )$, where $d_a$ = apparent dip; $d_t$ = true dip; $S_{xs}$ = ice direction; and $S_b$ = mean bedding strike. Notably, ($S_{xs} - S_b$) was converted to an absolute number. A negative apparent dip is possible, which means that palaeo-ice flow direction was up-dip, not down-dip.

## 4. Results

An overview of bedform data is presented in Table 1, with photographs from each study area shown in Figures 4 and 5. Table 2 presents structural bedrock data, and Figure 6 presents idealised schematic diagrams of bedforms from each study area.

### *4.1. Karrat Island subarea 1 (KA1)*

Bedrock in KA1 is predominantly metagreywacke. Beds are 5-30 cm thick, and bedding plane geometries are tightly clustered, striking SSW with an average dip angle of 42° (Fig. 7e). Two distinct

joint systems strike WNW and SW (Fig. 7e), with a mean dip of 74° and 9 joints $m^{-2}$. Fifty bedforms were measured in KA1: 6 meso-scale whalebacks and 44 meso-scale roches moutonnées. Bedforms range from 1.9 to 23.0 m in length, 1.6 to 4.0 m in width, and 0.9 to 9.0 m in height, giving a mean elongation ratio (ELR) of 2.52:1. Length:height ratios are 7.6, reflecting the relatively low relief, long cross profile of these classic roches moutonnées forms. The $r^2$ values shown in Figure 7 demonstrate weak correlations between bedform variables in KA1. Length and width show a weak positive correlation, with some bedforms becoming wider as they become longer. Height appears to have no correlation with bedform length ($r^2$ = 0.001), but shows a weak to moderate correlation with bedform width ($r^2$ = 0.486). Thus, taller bedforms are also wider, not longer. Throughout KA1, bedforms are well developed but display some fragmentation and weathering across their surface. Roches moutonnées display abrasion on stoss sides and display plucking on middle and lee slopes, producing south westerly facing plucked sides (e.g., Figure 4b). Whalebacks are poorly developed. Transverse wavelengths are up to 20 m, with densities of 190 – 240 bedforms $km^{-2}$. Striae directions are tightly clustered, indicating ice flow at 21 - 201° (Fig. 8), in broad accordance with mean bedform long axis orientation.

255 **Table 1.** Key morphological features of the bedforms mapped in this study from all four subareas.

256 See Figure 2 for area location. The key highlights the units used in the table.

| Subarea | Alt. range | RM (n) | WB (n) | Long axis | Striae | Min. L | Max. L | Min. W | Max. W | Min. H | Max. H |
|---|---|---|---|---|---|---|---|---|---|---|---|
| KA1 | 200-280 | 44 | 6 | 220 | 201 | 1.9 | 23.0 | 1.6 | 4.0 | 0.9 | 9.0 |
| KA2i | 200-300 | 20 | 0 | 175 | 265 | 0.8 | 13.2 | 1.5 | 15.0 | 0.7 | 4.4 |
| KA2ii | 200-300 | 30 | 0 | 185 | 212/268 | 0.8 | 11.1 | 0.9 | 10.0 | 0.6 | 1.7 |
| IN1 | 100-270 | 9 | 41 | 243 | 244 | 4.1 | 72.0 | 0.7 | 18.9 | 0.2 | 7.6 |
| IN2 | 100-250 | 5 | 25 | 266 | 225 | 7.5 | 96.0 | 1.0 | 12.0 | 0.9 | 3.3 |

257

| Subarea | ELR | L:H ratio | H:W ratio | Bedf. dens. | TW |
|---|---|---|---|---|---|
| KA1 | 2.52 | 7.61 | 0.39 | 192-240 | 20 |
| KA2i | 0.81 | 3.63 | 0.27 | 144-168 | 40 |
| KA2ii | 0.88 | 3.15 | 0.26 | 144-168 | 40 |
| IN1 | 4.79 | 21.37 | 0.35 | 160-190 | 12 |
| IN2 | 8.42 | 19.84 | 0.45 | 160-190 | 12 |

258

| **Key** | | | |
|---|---|---|---|
| RM (n) | *Number of roches moutonnées sampled* | Min. H | *Minimum bedform height in metres* |
| WB (n) | *Number of whalebacks sampled* | Max. H | *Maximum bedform length in metres* |
| Long axis | *Mean bedform long axis in degrees* | ELR | *Elongation ratio* |
| Striae | *Mean striae orientation in degrees* | L:H Ratio | *Ratio of bedform length to height* |
| Min. L | *Minimum bedform length in metres* | H:W Ratio | *Ratio of bedform height to width* |
| Max. L | *Maximum bedform length in metres* | Bedf. dens. | *Average bedform density per km2* |
| Min. W | *Minimum bedform width in metres* | TW | *Average transverse wavelength* |
| Max. W | *Maximum bedform length in metres* | | |

259

260 **Table 2.** Bedding features measured for each sub area, include mean strike and dip (with 1σ standard

261 deviations), and apparent dip.

| Subarea | Bedding strike | Std. dev. (1σ) | Bedding dip | Std. dev. (1σ) | Joint density ($m^{-2}$) | Apparent dip ($d_a$) (°) |
|---|---|---|---|---|---|---|
| KA1 | 196.4 | 15.5 | 40.6 | 12.2 | 9 | 3.9 |
| KA2i | 189.9 | 9.3 | 51.0 | 12.8 | 8 | 50.0 |
| KA2ii | 189.9 | 9.3 | 51.0 | 12.8 | 8 | 24.8[a] |
| KA2ii | 189.9 | 9.3 | 51.0 | 12.8 | 8 | 50.4[b] |
| IN1 | 237.2 | 9.3 | 23.0 | 3.6 | 5 | 2.9 |
| IN2 | 234.8 | 7.1 | 21.7 | 2.5 | 4 | 3.9 |

262 [a]Using striae direction 212° (see Table 1).

263 [b]Using striae direction 268° (see Table 1).

264

### *4.2. Karrat Island subarea 2 (KA2)*

As in KA1, bedrock in KA2 is mainly metagreywacke with some politic schist, though this was not seen on bedform surfaces. Bedding planes are tightly clustered; striking SSW with a mean dip of 51° (Fig. 7). Subvertical joint systems strike S and W, with 8 joints $m^{-2}$. Though the area was subdivided into KA2i and KA2ii, exposed bedrock was indistinguishable across KA2. Throughout KA2, bedforms are characterised by small, individual, rectilinear, meso-scale roches moutonnées (cf. Roberts and Long, 2005). In comparison to KA1, bedforms display less evidence of abrasion on their stoss surfaces. Plucked faces are present in KA2, but they are sloping (Fig. 4d), in contrast to the stepped lee side plucked faces of KA1. Bedforms display a transverse wavelength of 40 m and densities of 144 - 168 bedforms $km^{-2}$. After field observations (based upon variations in striae direction and number of plucked faces), it was decided that bedforms in KA2 represent two distinct bedform populations. As a result KA2 was subdivided into KA2i and KA2ii (see Figure 2a). Comparison of the morphometric measurements from KA1 and KA2 demonstrate that bedforms from these areas lie in three distinctly different populations (Figs. 7b-d), with bedforms in KA2 shorter, wider, and higher than those in KA1.

Striae on roches moutonnées in KA2i (*n* = 40) display evidence for unidirectional ice flow (85 - 265°) (Figs. 2a and 8; Table 1), almost perpendicular to bedform long axis orientation (175 - 355°). Roches moutonnées were short (0.8 - 13.2 m) and wide (1.5 - 15.0 m), resulting in mean ELRs of 0.8:1. Plucked faces are orientated west, concordant with the reconstructed ice flow direction and bedding plane and joint directions. Westerly plucked faces are glacially abraded (Fig. 4d), with faces conformable to bedding plane orientation.

Bedforms within KA2ii (*n* = 10) display evidence for two distinct phases of cross-cutting ice flow, 1 (32 - 212°) and 2 (88 - 268°) (Fig. 8; Table 1). Mean bedform long axis orientation is 10 - 190°,

290 oblique to the striae direction 1 (32 - 212°), and perpendicular to striae direction 2 (88 - 268°).
291 Within KA2ii, the striae show a cross-cutting relationship, with the 88 - 268° set appearing
292 superimposed upon the 32 - 212° set, suggesting switching of ice direction over the subarea.
293 Bedforms were of similar length to those from KA2i (0.80 – 11.10 m), but narrower (0.90 – 10.00 m),
294 with mean ELRs of 0.88:1. Bedforms from KA2ii display abraded lee side faces and double plucked
295 faces, oriented west (268 – 277°) and south-southwest (185 - 215°), broadly concordant with striae
296 directions. As in KA2i, west plucked faces were glacially abraded and conformable with bedding
297 plane dip and strike. In contrast to this, SSW-facing plucked faces are oblique to bedding plane and
298 to primary joint orientations and display blocky, stepped faces.
299
300 Bedform length:height ratios in KA2i are 3.63, and 3.15 in KA2ii, indicating lower relief bedforms in
301 KA2ii. However, bedforms from KA2ii show far less variation in height compared to width, reaching
302 a maximum height of 1.70 m. Throughout KA2, $r^2$ values reveal weak correlations between bedform
303 characteristics. Bedform width has no relationship to either bedform height ($r^2$ = 0.008) or length ($r^2$
304 = 0.045). A weak positive relationship exists between bedform length and height, suggesting that
305 some longer bedforms are taller, not wider.
306
307 *4.3. Ingia subarea 1 (IN1)*
308 Bedrock in IN1 is characterised by thinly bedded (5-20 cm) metagreywacke, striking SW with an
309 average dip of 22° (Fig. 9). Well-developed joint systems strike SW and SSE, with an average dip of
310 72°, and joint density of 5 joints $m^{-2}$. In places the metagreywacke contained massive bands of
311 quartzite up to 50 cm thick. Bedforms in IN1 are dominated by poorly developed meso-scale
312 whalebacks (*n* = 41) (cf. Roberts and Long, 2005), with some meso-roches moutonnées (*n* = 9).
313 Occasional microscale whalebacks were superimposed upon the larger bedforms, forming crude
314 whaleback swales. Swales are dense groups (or swarms) of whalebacks or roches moutonnées,

315 often superimposed upon one another (cf. Roberts and Long, 2005). Bedform long axis orientations
316 are tightly clustered at 74 - 254°. Bedforms are 4.1 – 72.0 m in length, 0.7 - 18.9 m in width, and 0.2
317 - 7.6 m in height (Figs. 9a-d). Mean elongation ratio (ELR) was 4.79:1. Evidence of abrasion is
318 present on the stoss and lee sides of all whalebacks, and lee side plucking is recorded on roches
319 moutonnées. All bedforms (whalebacks and roches moutonnées) also display plucking on their
320 lateral, south eastern faces (Figs. 5c and d). As a result, the bedforms were highly asymmetrical in
321 transverse profile. Transverse wavelength is 12 m, with a mean density of 160-190 bedforms $km^{-2}$.
322 Throughout IN1 striae are consistent, indicating a NE-SW (63 -243**°**) ice flow direction, subparallel to
323 fjord axis/thalweg. All relationships between bedform dimensions show weak relationships in IN2,
324 with $r^2$ values from 0.131 (width vs. height) to 0.290 (length vs. height) (Fig. 9).
325
326 *4.4. Ingia subarea 2 (IN2)*
327 The metagreywacke found in IN2 is lithologically comparable to bedrock in IN1. It is thinly bedded,
328 with beds reaching 20 cm thick. Bedding planes strike WSW with a mean dip of 22° (Fig. 9e). Joint
329 systems are well developed and strike SW and S, with an average dip of 62° (Fig. 9e) and joint
330 density of 4 joints $m^{-2}$ (Table 1). The metagreywacke contained bands of quartzite up to 50 cm thick
331 in places.
332
333 As in IN1, bedforms are characterised by poorly developed meso-scale whalebacks (*n* = 25) (cf.
334 Roberts and Long, 2005) with occasional smaller bedforms superimposed upon them. Bedform
335 cross-profile throughout IN2 is highly asymmetrical. Rare roches moutonnées (*n* = 5) were recorded.
336 Bedform ELRs from IN2 (8.42:1) are the highest in this study. Glacial polish is evident on stoss and
337 lee positions across bedforms, and where present, plucking is focused along the lateral, southern
338 flanks. The transverse wavelength of the bedform ridges is 12 m, giving an average density of 160-
339 190 bedforms $km^{-2}$. As in IN1, at site IN2 striae show that palaeo-ice flow was 45 - 225**°**, comparable

to the mean orientation of bedform long axes of 86 - 266° (Table 1). Striae were very rare, resulting in 10 measurements from IN1 and 12 from IN2. Ratios of length:height are 21.37 and 19.84 for IN1 and IN2, respectively; and height:width ratios are 0.35 and 0.45. Combined with the similarity in long axis orientation, this demonstrates that, in contrast to the distinct populations of KA1 and KA2, IN1 and IN2 represent a similar bedform population (Figs. 9b-d). Overall, $r^2$ values from IN2 are the highest of all subareas. Relationships between length and width ($r^2$ = 0.382) and length and height ($r^2$ = 0.201) remain relatively weak, but a weak-to-moderate positive correlation is found between width and height ($r^2$ = 0.477).

## 5. Discussion

### *5.1. Bedform relationship to ice flow*

The results appear directly analogous to those reported from other west Greenland palaeo-ice stream beds (Roberts and Long, 2005; Roberts et al., 2010), with low ELRs (2.8 - 3.7:1) and high bedform density (> 200 bedforms/km$^2$). Evidence for abrasion and plucking was found in all subareas, but in varying degrees of significance. It is generally thought that plucking is the more efficient agent of bedrock erosion (Briner and Swanson, 1998; Dühnforth et al., 2010). However, others have suggested that this is a generalisation (Krabbendam and Glasser, 2011), with erosional efficiency strongly dependent on local bedrock properties and structures, meaning that small variations in bedding structure result in large changes in erosion type. Owing to the absence of empirical data regarding the amount of erosion from this study, conclusions into the relative efficiency of either erosion method cannot be made.

Based upon regional geomorphological evidence (Lane et al., 2014), all field sites in this study would have been covered by 700 - 1000 m of ice during the last glaciation. Palaeo-ice flow velocities through Rink-Karrat and Ingia Fjord are assumed to have been high because of ice streaming through

365 the over-deepened Igdlorssuit and Uummannaq troughs (Ó Cofaigh et al., 2013; Roberts et al.,
366 2013). Striae show evidence for unidirectional ice flow (21 - 201°), sub-parallel to mean bedform
367 long axis (Table 1; Figure 8), and so bedforms in KA1 show a clear relationship to palaeo-ice flow
368 direction. Roches moutonnées show clear evidence of stoss side abrasion and extensive plucked
369 southwest-facing lee side faces – consistent with ice flow direction. In KA2i, unidirectional ice flow
370 (85 - 265°) was perpendicular to bedding strike, forming short rectilinear bedforms with abraded
371 stoss sides and westerly plucked lee side faces. Two clear phases of ice flow are recorded for KA2ii
372 (32 - 212° and 88 - 268°; Table 1; Figure 8). Because of the cross-cutting relationship mentioned in
373 section 4.2, all striae are assumed to represent the deglacial phase of ice flow across Karrat Island,
374 with the 32 - 212° formed first, overprinted by the 88 - 268° set as ice became topographically
375 constrained during deglaciation. The ELRs vary between KA1 and KA2i/KA2ii (2.52:1 and
376 0.80:1/0.88:1, respectively). However, given their close proximity (< 1.5 km), it is unlikely that ice
377 thickness and basal thermal conditions were significantly different to have altered bedform
378 geometry.
379
380 Bedform long axes in IN1 and IN2 are subparallel to palaeo-ice flow, suggesting that bedforms
381 represent a similar response to their palaeoglaciological conditions to bedforms in KA1. Despite a
382 uniform ice flow direction as recorded in striae over the two areas (64 - 244°), bedform long axes
383 show a small switch from 74 - 254° (IN1) to 86 - 266° (IN2). It is likely that this change in long axis is
384 because of the variation in ice flow direction associated with ice flow bending around the
385 topographic obstacle of the peninsula, as well as the bend within Ingia Fjord. As opposed to the
386 dominance of roches moutonnées in KA1 and KA2 (94 out of 100), 66 of 80 bedforms in IN1 and IN2
387 are whalebacks. Previously it has been suggested that whalebacks are formed through cavity
388 suppression beneath thick, fast-flowing ice (Evans, 1996). However, the southeast flanks of the

389 whaleback forms have undergone lateral plucking, a process requiring the presence of sub-glacial
390 cavities.
391
392 Ice flow direction has exerted the main control upon bedform formation indicated by the orientation
393 of bedform long axes and plucked faces. The multidirectional ice flow in KA2ii has caused the
394 development of dual plucked lee face orientations and bedforms with low ELRs, as reported in a
395 number of other studies (e.g., Roberts and Long, 2005; Roberts et al., 2010). Apparently, therefore,
396 bedforms in areas of unidirectional ice flow (KA1, KA2i, IN1, and IN2) display higher ELRs. This is a
397 result of a single ice flow direction promoting the development of elongate bedforms, as structural
398 weaknesses can be continuously exploited. In contrast, multidirectional ice flow is able to erode
399 variably oriented structural weaknesses with high angles, forcing elongation ratios to remain low.
400 Although this hypothesis is applicable for most areas in this study, it does not apply to KA2ii, where
401 bedforms are extremely short, with ELRs < 1:1, despite unidirectional ice flow and comparable
402 palaeo-ice thicknesses to other subareas.
403
404 *5.2. Bedform relationship to geological structure*
405 Subglacial bedform geometry is known to be strongly controlled by bedrock structure (Gordon,
406 1981; Roberts and Long, 2005; Dühnforth et al., 2010; Krabbendam and Glasser, 2011; Hooyer et al.,
407 2012). As described above, bedding plane strike, joint orientation and joint spacing vary greatly
408 between Karrat Island and Ingia (Figs. 7and 9; Table 2), and these differences have exerted control
409 on bedform morphology.
410
411 In KA1, KA2i, and KA2ii, bedding plane and joint characteristics have had a demonstrable impact
412 upon bedform properties. In KA1 the primary joint set is subvertical and strikes WNW, orthogonal to
413 palaeo-ice flow direction (Fig. 6), facilitating widespread lee side plucking of bedding plane and joint

414 defined blocks. In KA1 bedform width is likely to have been controlled by joints sub-parallel to ice
415 flow (striking SW) and moderately dipping bedding planes striking SSW – acting as lines of weakness
416 along which ice has been able to erode. Plucked lee side development in KA2i has been facilitated
417 by extensive, well-developed, SSW-striking bedding planes and S-striking joint systems,
418 perpendicular to palaeo-ice flow direction (85 - 265°), and dipping down-ice. The orientation and
419 steep bedding plane dip is thought to have facilitated ice-bed separation in the lee sides of
420 bedforms, allowing the exploitation of bedding planes and joints subparallel to palaeo-ice flow by
421 plucking directly along metagreywacke beds. This process has generated the down-ice sloping lee
422 side plucked faces. The less extensive east to west joint system has aided plucking of blocks
423 bounded by down-ice dipping bedding surfaces, N-S and E-W trending joints. The low density of this
424 E-W joint set allowed bedforms to maintain their large width and consequently low ELRs. The wide
425 spacing of the joints provided fewer points of structural weakness at which erosion can be focused
426 to breach the laterally extensive metagreywacke beds. Thus, the low ELRs (~0.8:1) of bedforms in
427 KA2i are a direct result of bedrock structure.
428
429 Bedforms in KA2ii exhibit multiple plucked faces, recording plucking in response to ice flow from the
430 east and northeast. The striae chronology outlined above is assumed to record deglaciation across
431 Karrat Island. While bedform development is assumed to be a continuous process, the bedforms
432 observed in KA2ii are most simply related to the two striae directions observed. Though uncertain,
433 the chronology proposed above based on cross-cutting striae (see section 5.1) and on increasing
434 topographic control on ice flow during deglaciation. If the chronology is incorrect, the events would
435 be reversed, making little difference to the landform development model below. During NE-SW
436 directed ice flow SSW- and S-facing faces were plucked, with block removal facilitated by E-W and N-
437 S trending joints and by SSW-striking bedding planes. This phase of ice flow was oblique to joint
438 orientation, and the resulting plucked faces are not well developed. Subsequently, E-W ice flow

caused plucking of westerly oriented faces, again removing blocks bounded by the E-W and N-S trending joints, but with block removal in a westerly direction. Roberts et al. (2010) reported bedforms formed through bidirectional ice flow, transverse and subparallel to the bedding plane strike and dip, directly comparable to KA2ii. As in KA2ii, the distinct geological and bidirectional ice flows have produced short, wide bedforms with low ELRs and multiple plucked faces (Roberts et al., 2010).

In IN1 and IN2, bedrock structure has exerted a strong control upon bedform type (roches moutonnées/whaleback), length, width and orientation. Although little lee side plucking was documented at IN1 and IN2, almost all bedforms displayed evidence for extensive block removal from their steep, lateral SE faces (Figs. 5D, E). This plucking has been facilitated by exploitation of the exposed ends of SW-striking bedding planes, with block removal occurring along subvertical joints. Bedforms on Ingia are dominated by whalebacks (66 out of 80). As discussed above, their presence and their abundance is unlikely to be a function of ice flow as ice flow characteristics between Ingia and Karrat Island are similar. Instead it is due to bedrock properties. They display ubiquitous stoss and lee side abrasion and little evidence of lee side plucking, despite the presence of joints running transverse to palaeo-ice flow. This absence of evidence of lee side plucking is interpreted to be the result of three factors. Firstly, strike of bedding planes and the majority of joints are sub-parallel to palaeo-ice flow, with low transverse joint density (~2 joints/$m^2$ in comparison to 6 transverse joints/$m^2$ in KA1 and KA2). Secondly, a number of bedforms display thick (30-50 cm) bands of quartzite, interbedded with metagreywacke. In places these cap the bedforms or outcrop at the bedform surface. The crystalline quartzite contains far fewer transverse structural weaknesses (~1 joints/$m^2$) than metagreywacke and is harder and more resistant to erosion. Therefore, where present, quartzite has limited plucking creating abraded stoss and lee side forms (whalebacks). Thirdly, the thin bedding planes in IN1 and IN2 have an apparent down-ice dip of 2.88

– 3.87° relative to palaeo-ice flow (see section 5.3 for a discussion of this). As the metagreywacke in IN1 and IN2 is thinly bedded (5-15 cm), and thus less resistant to subglacial erosion than thicker bedded metagreywacke, erosion removes material along the thin beds. This therefore prevents the development of a classic stepped lee side face, preserving the sloped face and whaleback form.

A similar style of bedrock plucking to that recorded on the lateral flanks of bedforms in IN1 and IN2 has been outlined by Krabbendam and Bradwell (2011), termed lateral plucking. In their study, erosion by this process led to the development of a series of negative relief megagroove features, not the positive relief bedforms observed in the present study (Krabbendam and Bradwell, 2011). During lateral plucking, cavities develop on steep vertical surfaces, lateral to the main bedform surface and approximately parallel to the long axis. Erosion occurs along joints and bedding planes (allowing block loosening and translocation) about a vertical axis, leading to erosion perpendicular to ice flow direction (Krabbendam and Bradwell, 2011). A relative absence of protuberances on megagroove floors, or roches moutonnées/whaleback upper surfaces, led to the suggestion that erosion was abrasion-dominated (Krabbendam and Bradwell, 2011). This is despite the variable bedding dip (5-40°) reported by Krabbendam and Bradwell (2011), which is likely to have exposed lines of weakness to plucking. In IN1 and IN2, lateral plucking has acted to control bedform width through rock removal from lateral flanks. Bedforms in IN1 and IN2 only display this on south eastern flanks where exposed bedding planes can be readily exploited. It appears that the type of plucking (lee side or lateral) and the resultant landform (positive bedforms or negative grooves) are highly dependent upon local geological structure (e.g., bedding plane dip, bed thickness, joint orientation, joint spacing) and probably the form of the surface prior to the most recent glaciation.

The distinct offset between plucked-face orientation and palaeo-ice flow direction (which was observed in KA2i, KA2ii, IN1, and IN2) has also been reported by other studies (Gordon, 1981; Rea

and Whalley, 1996; Krabbendam and Bradwell, 2011; Hooyer et al., 2012). Plucking is facilitated by pre-glacial bedding planes and joints and by bedrock rock bridges (Hooyer et al., 2012) (Fig. 10). Block removal occurs when rock bridges between joint-bounded blocks fail; meaning that plucked-faced distribution preferentially follows joint orientation as opposed to ice flow direction (Hooyer et al., 2012).

### *5.3. Importance of apparent bedding dip relative to ice flow direction*

Bedding plane dip angle was outlined by Gordon (1981) as one of the factors affecting bedform characteristics and was considered by Rea and Whalley (1996) in their plucking calculation. More recently, Krabbendam and Bradwell (2011) discussed its impact upon lee side plucking. Over a regional scale, Kelly et al. (2014) demonstrated the importance of bedding plane dip on the prevalence of glacial steps, scour surfaces, and overdeepenings. From this study, the strike and dip of bedding *relative* to palaeo-ice flow direction(s) ($d_a$) is a significant factor controlling bedform relief and morphology (Table 2). We have calculated this as apparent dip, as outlined above (section 3). When compared to bedform morphometry, a relationship exists between measured ELR and calculated apparent dip, with high $d_a$ correlated to low ELR. This preliminary data set provides an important insight into the potential relationships between apparent dip and bedform morphometry. While the interpretations are currently tentative, these relationships are discussed below.

Based on these data, likely bedform characteristics under different apparent bedding plane dip configurations can be predicted (Fig. 11). When $d_a$ is low relative to palaeo-ice flow (either up- or down-ice), resultant bedforms are low in relief and amplitude, with high ELRs (e.g., IN1 and IN2) (Fig. 11). Low $d_a$, either perpendicular or parallel to flow, favours low form drag (Fig. 11), offering a pathway of low resistance for basal ice. This leads to the maintenance of a bed with low relief and roughness, reducing the difference in stress between stoss to lee faces, decreasing the likelihood of

quarrying/plucking, and promoting the development of long bedforms. This low form drag is particularly likely to occur in regions of shallow dipping up-ice bedding planes. Here, bedforms produced through glacial erosion will be roche moutonnée in form, with high ELRs (Fig. 11), the smooth up-ice surfaces promoting low bed roughness. Bedforms in areas of shallow, down-ice dipping bedding planes will be whaleback in form, also with long ELR (Fig. 11). In this setting the top surfaces of bedforms have the potential to detach as a slab. In contrast, if bedding plane dip relative to palaeo-ice flow is high, resultant bedforms have larger amplitudes and display low ELRs (e.g., KA2), increasing along bed stresses leading to the formation of high relief roches moutonnées through widespread lee side plucking (Fig. 11). Such settings have high roughness leading to high basal drag. If bedding planes dip up-ice, lee side cavity formation and subsequent plucking is encouraged, producing classic roches moutonnées (Fig. 11) (Benn and Evans, 2010). Conversely, if the bedding planes dip down-ice, roches moutonnées with smooth non stepped lee faces form (Fig. 11) (e.g., KA2i). Resultant bedforms are likely to have low ELRs and high amplitude. Variability in $d_a$ relative to ice flow only controls bedform length, so the development of high ELRs is dependent upon bedform. On a smaller scale, joints are likely to act in a similar way to bedding planes. Thus bedding plane and joint orientation relative to palaeo-ice flow is also able to control bed roughness on the scale of a single bedform, and multiple structures orientated at high angles to palaeo-ice flow will encourage quarrying. However, these finer scale effects cannot be resolved using data from this study. Although the difference in dip angle has been referred to here as 'low' and 'high', in reality ice flow relative to bedding plane dip and bedform properties (ELR/bedform type) lie on a continuum. Increases in the dip angle are therefore hypothesised to gradually decrease bedform length until a dip close to 90˚ is reached.

## 6. Conclusion

This study has investigated the controls on bedrock bedform development in two neighbouring fjords in central West Greenland. These lie in the upstream reaches of the palaeo-UIS and are believed to have experienced topographically constrained, fast ice flow during the LGM. Reconstructions have suggested that palaeoglaciological conditions were similar for all sites in the study, being characterised by thick, fast-flowing ice moving over a rigid bedrock bed. Palaeo-ice flow direction has exerted a first-order control on bedform orientation, with the majority of areas displaying bedform long axes sub-parallel to ice flow direction, as indicated by striae evidence. Bedforms in areas that experienced multiple ice flow directions (KA2ii) display multiple plucked faces, resulting in widespread bedform shortening, as reported in other studies. In contrast, subareas that experienced unidirectional ice flow displayed longer bedforms. However, the variability in bedform morphology cannot be explained solely by palaeo-glacier dynamics. Instead, pre-glacial joint and bedding plane orientations have controlled bedform width and height through plucking. Bedforms on Karrat and Ingia displayed evidence for areally extensive abrasion and plucking.

Elongation ratios varied in this study between 0.81:1 and 8.42:1. Owing to the uniformity of hypothesised palaeoglaciological conditions across the study areas, bedform ELR appears to be controlled by the apparent dip ($d_a$). Shallow $d_a$ promotes low bed roughness and high ELRs, whereas steep $d_a$ encourages high roughness and low ELRs. Whaleback bedforms were found in areas of shallow, down-ice dipping bedrock, with low joint densities. This has resulted in plucking along bedding planes, with some abrasion of lee sides, creating whaleback forms. The results of this further highlight the need for further investigation on bedrock bedform characteristics before using them to investigate palaeo-ice flow dynamics.

**Acknowledgements**

This work was supported by the Department of Geography (Durham University), the Department of Geography and the Environment (University of Aberdeen), the Royal Geographical Society-IBG, and the Carnegie Trust for the Universities of Scotland. Thanks to Arne Neumann, Birte Ørum, and Barbara Stroem-Baris for logistical support during fieldwork. Reproduced aerial photographs were provided by Kort and Matrikelstyrelsen. Arjen Stroeven, Emrys Phillips, two anonymous reviewers, and the editor are thanked for their comments, which assisted in improving and clarifying this manuscript.

572 ***References***


573 Benn, D., Evans, D.J.A., 2010. Glaciers and Glaciation. Hodder Education, London.

574 Boulton, G.S., 1974. Processes and patterns of glacial erosion. In: D.R. Coates (Ed.), Glacial
575 Geomorphology. State University of New York, New York, pp. 41-56.

576 Bradwell, T., Stoker, M., Krabbendam, M., 2008. Megagrooves and streamlined bedrock in NW
577 Scotland: The role of ice streams in landscape evolution. Geomorphology, 97, 22.

578 Briner, J.P., Swanson, T.W., 1998. Using inherited cosmogenic Cl-36 to constrain glacial erosion rates
579 of the Cordilleran ice sheet. Geology, 26(1), 3-6.

580 Canals, M., Casamor, J.L., Urgeles, R., Calafat, A.M., Domack, E.W., Baraza, J., Farran, M., De Batist,
581 M., 2002. Seafloor evidence of a subglacial sedimentary system off the northern Antarctic
582 Peninsula. Geology, 30(7), 603-606.

583 Clark, C.D., 1993. Mega-scale glacial lineations and cross-cutting ice-flow landforms. Earth Surface
584 Processes and Landforms, 18(1), 1-29.

585 Dowdeswell, J., Hogan, K., Ó Cofaigh, C., Fugelli, E., Evans, J., Noormets, R., 2014. Late Quaternary ice
586 flow in a West Greenland fjord and cross-shelf trough system: submarine landforms from
587 Rink Isbrae to Uummannaq shelf and slope. Quaternary Science Reviews, 92, 292-309.

588 Dowdeswell, J., Ottesen, D., Evans, J., Cofaigh, C.Ó., Anderson, J., 2008. Submarine glacial landforms
589 and rates of ice-stream collapse. Geology, 36(10), 819-822.

590 Dühnforth, M., Anderson, R.S., Ward, D., Stock, G.M., 2010. Bedrock fracture control of glacial
591 erosion processes and rates. Geology, 38(5), 423-427.

592 Evans, I.S., 1996. Abraded rock landforms (whalebacks) developed under ice streams in mountain
593 areas. Annals of Glaciology, 22, 9-15.

594 Evans, J., Ó Cofaigh, C., Dowdeswell, J.A., Wadhams, P., 2009. Marine geophysical evidence for
595 former expansion and flow of the Greenland Ice Sheet across the north-east Greenland
596 continental shelf. Journal of Quaternary Science, 24(3), 279-293.

597 Garde, A.A., Steenfelt, A., 1999. Precambrian geology of Nuussuaq and the area north-east of Disko
598 Bugt, West Greenland. In: F. Kalsbeek (Ed.), Precambrian geology of the Disko Bugt region,
599 West Greenland. GEUS, Copenhagen, pp. 6-40.

600 Glasser, N.F., Bennett, M.R., 2004. Glacial erosional landforms: origins and significance for
601 palaeoglaciology. Progress in Physical Geography, 28(1), 43-75.

602 Glasser, N.F., Warren, C.R., 1990. Medium Scale Landforms of Glacial Erosion in South Greenland;
603 Process and Form Geografiska Annaler Series a-Physical Geography, 72, 5.

604 Gordon, J.E., 1981. Ice-Scoured Topography and Its Relationships to Bedrock Structure and Ice
605 Movement in Parts of Northern Scotland and West Greenland. Geografiska Annaler. Series
606 A, Physical Geography, 63(1/2), 55-65.

607 Graham, A.G.C., Larter, R.D., Gohl, K., Hillenbrand, C.-D., Smith, J.A., Kuhn, G., 2009. Bedform
608 signature of a West Antarctic palaeo-ice stream reveals a multi-temporal record of flow and
609 substrate control. Quaternary Science Reviews, 28(25–26), 2774-2793.

610 Hallet, B., 1996. Glacial quarrying: A simple rheoretical model. Annals of Glaciology, 22, 1-8.

611 Henderson, G., Pulvertaft, T.C.R., 1987a. Descriptive text to geological map of Greenland 1:100 000,
612 Marmorilik 71 V.2 Agnete Syd, Nugatsiaq 71 V.2 Nord and Pangnertoˆq 72 V.2 Syd. Geol.
613 Survey Greenland, Copenhagen,.

614 Henderson, G., Pulvertaft, T.C.R., 1987b. Geological map of Greenland, 1:100 000, Mârmorilik 71 V.2
615 Syd, Nûgâtsiaq 71 V.2 Nord, Pangnertôq 72 V.2 Syd. In: G.S.o. Greenland (Ed.), Copenhagen.

616 Henriksen, N., Higgins, A.K., Kalsbeek, F., 2000. Greenland from Archaean to Quaternary Descriptive
617 text to the Geological map of Greenland,1:2 500 000. GEUS, Copenhagen.

618 Hindmarsh, R., 1996. Sliding of till over bedrock: scratching, polishing, comminution and kinematic-
619 wave theory. Annals of Glaciology, 22, 41-47.

620 Hogan, K.A., Dowdeswell, J.A., Noormets, R., Evans, J., Ó Cofaigh, C., Jakobsson, M., 2010. Submarine
621 landforms and ice-sheet flow in the Kvitøya Trough, northwestern Barents Sea. Quaternary
622 Science Reviews, 29(25–26), 3545-3562.
623 Hooyer, T.S., Cohen, D., Iverson, N.R., 2012. Control of glacial quarrying by bedrock joints.
624 Geomorphology, 153, 91-101.
625 Iverson, N.R., 1991. Morphology of glacial striae: implications for abrasion of glacier beds and fault
626 surfaces. Geological Society of America Bulletin, 103(10), 1308-1316.
627 Iverson, N.R., 2012. A theory of glacial quarrying for landscape evolution models. Geology, 40(8),
628 679-682.
629 Jansson, K.N., Stroeven, A.P., Kleman, J., 2003. Configuration and timing of Ungava Bay ice streams,
630 Labrador-Ungava, Canada. Boreas, 32, 256-263.
631 Kalsbeek, F., Pulvertaft, T.C.R., Nutman, A.P., 1998. Geochemistry, age and origin of metagreywackes
632 from the Palaeoproterozoic Karrat Group, Rinkian Belt, West Greenland. Precambrian
633 Research, 91(3–4), 383-399.
634 Kelly, M.H., Anders, A.M., Mitchell, S.G., 2014. Influence of Bedding Dip on Glacial Erosional
635 Landforms, Uinta Mountains, USA. Geografiska Annaler: Series A, Physical Geography.
636 King, E.C., Hindmarsh, R.C.A., Stokes, C.R., 2009. Formation of mega-scale glacial lineations observed
637 beneath a West Antarctic ice stream. Nature Geosci, 2(8), 585-588.
638 Kleman, J., Stroeven, A.P., Lundqvist, J., 2008. Patterns of Quaternary ice sheet erosion and
639 deposition in Fennoscandia and a theoretical framework for explanation. Geomorphology,
640 97(1-2), 73-90.
641 Krabbendam, M., Bradwell, T., 2011. Lateral plucking as a mechanism for elongate erosional glacial
642 bedforms: explaining megagrooves in Britain and Canada. Earth Surface Processes and
643 Landforms, 36(10), 1335-1349.
644 Krabbendam, M., Glasser, N., 2011. Glacial erosion and bedrock properties in NW Scotland: Abrasion
645 and plucking, hardness and joint spacing. Geomorphology, 130, 10.
646 Lane, T.P., Roberts, D.H., Rea, B.R., Ó Cofaigh, C., Vieli, A., Rodés, A., 2014. Controls upon the Last
647 Glacial Maximum deglaciation of the northern Uummannaq Ice Stream System, West
648 Greenland. Quaternary Science Reviews, 92, 324-344.
649 Lindstrom, E., 1988. Are roches moutonnees mainly preglacial forms? Geografiska Annaler: Series A,
650 Physical Geography, 70A, 323-322.
651 Lisle, R.J., 2004. Geological Structures and Maps Butterworth-Heinemann, UK.
652 Lowe, A.L., Anderson, J., 2002. Reconstruction of the West Antarctic ice sheet in Pine Island Bay
653 during the Last Glacial Maximum and its subsequent retreat history. Quaternary Science
654 Reviews, 21, 1879-1897.
655 MacAyeal, D., 1993. Binge/purge oscillations of the Laurentide ice sheet as a cause of the North
656 Atlantic's Heinrich events. Paleoceanography, 8(6), 775-784.
657 Ó Cofaigh, C., Dowdeswell, J.A., Jennings, A.E., Hogan, K.A., Kilfeather, A., Hiemstra, J.F., Noormets,
658 R., Evans, J., McCarthy, D.J., Andrews, J.T., Lloyd, J.M., Moros, M., 2013. An extensive and
659 dynamic ice sheet on the West Greenland shelf during the last glacial cycle. Geology, 41(2),
660 219-222.
661 Ó Cofaigh, C., Pudsey, C.J., Dowdeswell, J.A., Morris, P., 2002. Evolution of subglacial bedforms along
662 a paleo-ice stream, Antarctic Peninsula continental shelf. Geophys. Res. Lett., 29(8), 1199.
663 Ó Cofaigh, C., Taylor, J., Dowdeswell, J.A., Pudsey, C.J., 2003. Palaeo-ice streams, trough mouth fans
664 and high-latitude continental slope sedimentation. Boreas, 32(1), 37-55.
665 Ottesen, D., Stokes, C.R., Rise, L., Olsen, L., 2008. Quaternary ice-sheet dynamics and ice streaming
666 along the coastal parts of northern Norway. Quaternary Science Reviews, 27, 19.
667 Pedersen, G.K., Pulvertaft, T.C.R., 1992. The nonmarine Cretaceous of the West Greenland Basin,
668 onshore West Greenland. Cretaceous Research, 13(3), 263-272.

669 Phillips, E., Everest, J., Diaz-Doce, D., 2010. Bedrock controls on subglacial landform distribution and
670 geomorphological processes: Evidence from the Late Devensian Irish Sea Ice Stream.
671 Sedimentary Geology, 232(3–4), 98-118.
672 Rea, B., 2007. Glacial landforms, erosional features: Micro to macro-scale forms. In: S. Elias (Ed.),
673 Encyclopedia of Quaternary Science. Elsevier, Oxford, pp. 853-864.
674 Rea, B.R., Whalley, B.W., 1994. Subglacial observations from øksfjordjøkelen, North Norway. Earth
675 Surface Processes and Landforms, 19(7), 659-673.
676 Rea, B.R., Whalley, W.B., 1996. The role of bedrock topography, structure, ice dynamics and
677 preglacial weathering in controlling subglacial erosion beneath a high-latitude, maritime ice
678 field. Annals of Glaciology, 22, 121-125.
679 Roberts, D.H., Long, A.J., 2005. Streamlined bedrock terrain and fast ice flow, Jakobshavns Isbrae,
680 West Greenland: implications for ice stream and ice sheet dynamics. Boreas, 34(1), 25-42.
681 Roberts, D.H., Long, A.J., Davies, B.J., Simpson, M.J.R., Schnabel, C., 2010. Ice stream influence on
682 West Greenland Ice Sheet dynamics during the Last Glacial Maximum. Journal of Quaternary
683 Science, 25(6), 850-864.
684 Roberts, D.H., Rea, B.R., Lane, T.P., Schnabel, C., Rodes, A., 2013. New constraints on Greenland ice
685 sheet dynamics during the last glacial cycle: evidence from the Uummannaq ice stream
686 system. Journal of Geophysical Research: Earth Surface, 118(2), 23.
687 Sejrup, H.P., Larsen, E., Haflidason, H., Berstad, I.M., Hjelstuen, B.O., Jonsdottir, H.E., King, E.L.,
688 Landvik, J., Longva, O., Nygard, A., Ottesen, D., Raunholm, S., Rise, L., Stalsberg, K., 2003.
689 Configuration, history and impact of the Norwegian Channel Ice Stream. Boreas, 32(1), 18-
690 36.
691 Stokes, C.R., Clark, C.D., 1999. Geomorphological criteria for identifying Pleistocene ice streams.
692 Annals of Glaciology, 28, 67-79.
693 Stokes, C.R., Clark, C.D., 2001. Palaeo-ice streams. Quaternary Science Reviews, 20, 1437-1456.
694 Stokes, C.R., Clark, C.D., Darby, D.A., Hodgson, D.A., 2005. Late Pleistocene ice export events into the
695 Arctic Ocean from the M'Clure Strait ice stream, Canadian Arctic Archipelago. Global and
696 Planetary Change, 49(3), 139-162.
697 Stokes, C.R., Clark, C.D., Storrar, R., 2009. Major changes in ice stream dynamics during deglaciation
698 of the north-western margin of the Laurentide Ice Sheet. Quaternary Science Reviews, 28(7–
699 8), 721-738.
700 Sugden, D.E., 1974. Landscapes of glacial erosion in Greenland and their relationship to ice,
701 topographic and bedrock conditions. In: E.H. Brown, R.S. Waters (Eds.), Progress in
702 Geomorphology: Papers in honour of David L. Linton. Institute of British Geographers
703 Special Publication. No. 7. Institute of British Geographers, London, pp. 177-195.
704 Sugden, D.E., Glasser, N., Clapperton, C.M., 1992. Evolution of large roche moutonnees. Geografiska
705 Annaler: Series A, Physical Geography, 74 (A)(2-3), 253-264.

706

707

**Table 1.** Key morphological features of the bedforms mapped in this study from all four subareas.

See Figure 2 for area location. The key highlights the units used in the table.

| Subarea | Alt. range | RM (n) | WB (n) | Long axis | Striae | Min. L | Max. L | Min. W | Max. W | Min. H | Max. H |
|---|---|---|---|---|---|---|---|---|---|---|---|
| KA1 | 200-280 | 44 | 6 | 220 | 201 | 1.9 | 23.0 | 1.6 | 4.0 | 0.9 | 9.0 |
| KA2i | 200-300 | 20 | 0 | 175 | 265 | 0.8 | 13.2 | 1.5 | 15.0 | 0.7 | 4.4 |
| KA2ii | 200-300 | 30 | 0 | 185 | 212/268 | 0.8 | 11.1 | 0.9 | 10.0 | 0.6 | 1.7 |
| IN1 | 100-270 | 9 | 41 | 243 | 244 | 4.1 | 72.0 | 0.7 | 18.9 | 0.2 | 7.6 |
| IN2 | 100-250 | 5 | 25 | 266 | 225 | 7.5 | 96.0 | 1.0 | 12.0 | 0.9 | 3.3 |

| Subarea | ELR | L:H ratio | H:W ratio | Bedf. dens. | TW |
|---|---|---|---|---|---|
| KA1 | 2.52 | 7.61 | 0.39 | 192-240 | 20 |
| KA2i | 0.81 | 3.63 | 0.27 | 144-168 | 40 |
| KA2ii | 0.88 | 3.15 | 0.26 | 144-168 | 40 |
| IN1 | 4.79 | 21.37 | 0.35 | 160-190 | 12 |
| IN2 | 8.42 | 19.84 | 0.45 | 160-190 | 12 |

| **Key** | | | |
|---|---|---|---|
| RM (n) | *Number of roches moutonnées sampled* | Min. H | *Minimum bedform height in metres* |
| WB (n) | *Number of whalebacks sampled* | Max. H | *Maximum bedform length in metres* |
| Long axis | *Mean bedform long axis in degrees* | ELR | *Elongation ratio* |
| Striae | *Mean striae orientation in degrees* | L:H Ratio | *Ratio of bedform length to height* |
| Min. L | *Minimum bedform length in metres* | H:W Ratio | *Ratio of bedform height to width* |
| Max. L | *Maximum bedform length in metres* | Bedf. dens. | *Average bedform density per km2* |
| Min. W | *Minimum bedform width in metres* | TW | *Average transverse wavelength* |
| Max. W | *Maximum bedform length in metres* | | |

**Table 2.** Bedding features measured for each sub area, include mean strike and dip (with 1σ standard deviations), and apparent dip.

| Subarea | Bedding strike | Std. dev. (1σ) | Bedding dip | Std. dev. (1σ) | Joint density ($m^{-2}$) | Apparent dip ($d_a$) (°) |
|---|---|---|---|---|---|---|
| KA1 | 196.4 | 15.5 | 40.6 | 12.2 | 9 | 3.9 |
| KA2i | 189.9 | 9.3 | 51.0 | 12.8 | 8 | 50.0 |
| KA2ii | 189.9 | 9.3 | 51.0 | 12.8 | 8 | 24.8[a] |
| KA2ii | 189.9 | 9.3 | 51.0 | 12.8 | 8 | 50.4[b] |
| IN1 | 237.2 | 9.3 | 23.0 | 3.6 | 5 | 2.9 |
| IN2 | 234.8 | 7.1 | 21.7 | 2.5 | 4 | 3.9 |

[a]Using striae direction 212° (see Table 1).

[b]Using striae direction 268° (see Table 1).

**Figure Captions**

Click here to view linked References

**Fig. 1.** (A) Overview topographic map of the Uummannaq region. Altitudes have been extracted from ASTER data and ocean floor bathymetry is from IBCAO data (Jakobsson et al., 2012). Broad geological zones of bedrock are shown, separated by white dashed lines. These are: (1) Palaeogene basalts; (2) Palaeozoic-Mesozoic sediments; (3) Archean basement (adapted from Henderson, 1971); (B) enlargement of Karrat Island, showing local geology; (C) enlargement of the local geology in Ingia Fjord (from Henderson and Pulvertaft, 1987a; b).

**Fig. 2.** Aerial photographs from (A) Karrat Island and (B) the peninsula Ingia Fjord, with dashed boxes indicating study areas. Rose diagrams show striae measurements from specific sites across Karrat Island and Ingia peninsula. Average bedform long axes and secondary axes orientations are shown in white crosses.

**Fig. 3.** Schematic diagram of the calculation of the apparent bedding plane dip ($d_a$) when palaeo-ice flow direction is taken into account. Other variables are: $d_t$ = true dip; $S_{xs}$ = ice direction; $S_b$ = mean bedding strike.

**Fig. 4.** Photographs of bedforms from study sub-areas with long-axis orientations (grey arrows). White lines highlight bedform outlines for clarity when viewing: (A) aerial image showing locations of the photographs; (B) roche moutonnées from KA1, with abraded stoss sides and heavily plucked lee sides (left of image). Frequent striae were found across upper faces. Palaeo-ice flow right to left; (C) example of cross-cutting striae found within KA2ii; (D) short, rectilinear roche moutonnées from KA2ii. Multidirectional striae and plucked faces suggest multiple palaeo-ice flow directions.

**Fig. 5.** Photographs of bedforms from study sub-areas with long-axis orientations (grey arrows). White lines highlight bedform outlines for clarity when viewing: (A) aerial image showing locations of the photographs; (B) field of smooth whalebacks and occasional roche moutonnées in IN1: palaeo-ice flow from right to left of the image; (C) cross profile of clearly asymmetrical whalebacks from IN2 with palaeo-ice flow toward the camera. Little lee-side plucking is evident; (D) side view of a whaleback bedform in IN1. Gently dipping to sub horizontal bedding planes are evident, and the lee-side morphology of the bedform conforms to bedding plane dip. The bedform flank facing the camera displays clear evidence of block removal through 'lateral plucking'; (E) another view of the lateral face of a representative bedform from IN1, with lateral plucking, and the smoothed long-profile of the bedform visible.

**Fig. 6.** Schematic diagrams representative of the bedforms found in each sub-area of this study. Black lines represent bedding planes and grey dashed lines represent principle joint sets. This is a diagrammatic representation of bedform morphology, and bedding structures are not in precise locations.

**Fig. 7.** Bedform data from KA1 (black triangles) and KA2 (open squares): (A) scatter plot of width against length; (B) scatter plot of height against length; (C) scatter plot of elongation ratio (ELR) against length; (D) scatter plot of width against height; (E) bedding strike and joint dip orientation plotted in stereonets as poles to planes, with several planes to indicate dominant bedding direction.

**Fig. 8.** Striae data from all sub-areas plotted in rose diagrams. Note that striae in IN1 and IN2 were sparse, and poorly preserved on bedrock surfaces.

**Fig. 9.** Bedform data from IN1 (black triangles) and IN2 (open squares): (A) scatter plot of width against length for IN1 and IN2; (B) scatter plot of height against length for IN1 and IN2; (C) scatter plot of elongation ratio (ELR) against length for IN1 and IN2; (D) scatter plot of width against height for IN1 and IN2; (E) bedding strike and joint dip orientation plotted in stereonets as poles to planes, with several planes to indicate dominant bedding direction.

**Fig. 10.** Schematic diagram showing the development of bedforms in each sub-area, based on an idealised version of the joint and bedding systems. The schematic shows the planview of bedding structures, side profile of bedding plane dip, and planview of resultant bedforms.

**Fig. 11.** Model of bedform formation in regions of varied relative up- or down-ice bedding plane dip and hypothesised resulting bedforms. Black arrows represent ice flow direction. Green areas indicate surfaces dominated by glacial abrasion; red areas indicate surfaces dominated by lee-side plucking.

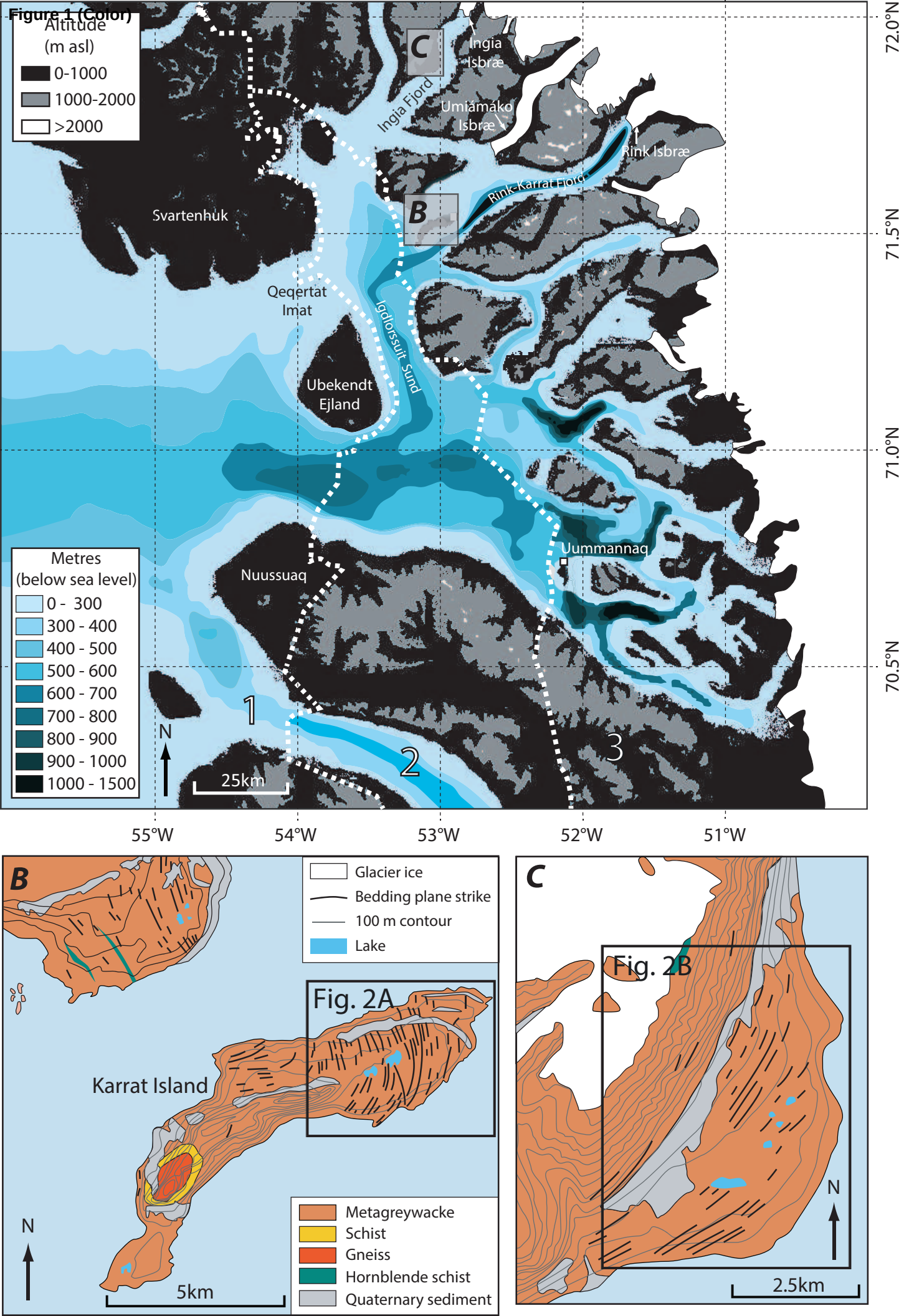
Figure 1 (Color)
Altitude (m asl)
0-1000
1000-2000
>2000
C
Ingia Isbræ
Ingia Fjord
Umiámáko Isbræ
Rink Isbræ
Rink-Karrat Fiord
B
Svartenhuk
Qeqertat Imat
Igdlorssuit Sund
Ubekendt Ejland
Uummannaq
Nuussuaq
1
2
3
N
25km
Metres (below sea level)
0 - 300
300 - 400
400 - 500
500 - 600
600 - 700
700 - 800
800 - 900
900 - 1000
1000 - 1500
72.0°N
71.5°N
71.0°N
70.5°N
55°W
54°W
53°W
52°W
51°W
B
Glacier ice
Bedding plane strike
100 m contour
Lake
Fig. 2A
Karrat Island
N
5km
Metagreywacke
Schist
Gneiss
Hornblende schist
Quaternary sediment
C
Fig. 2B
N
2.5km

**Figure 2 (Color)**

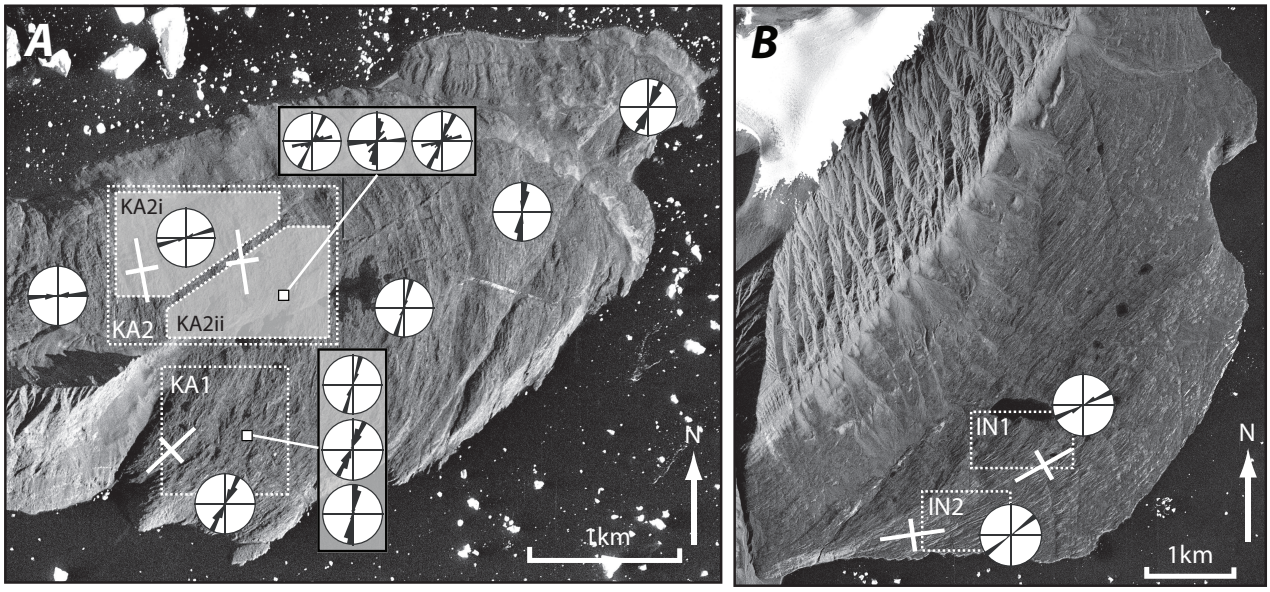

**Figure 4 (Color)**

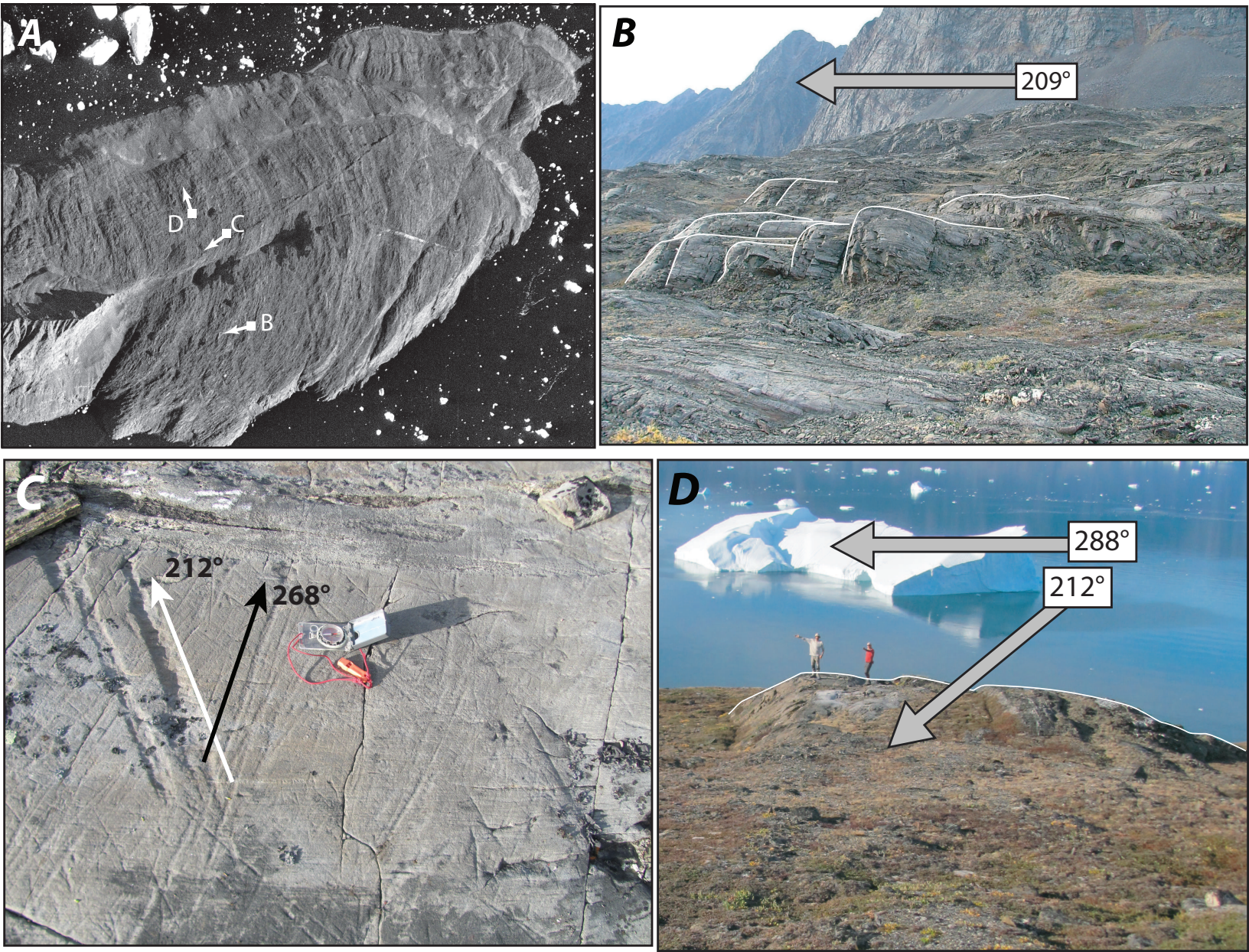

Figure 5 (Color)

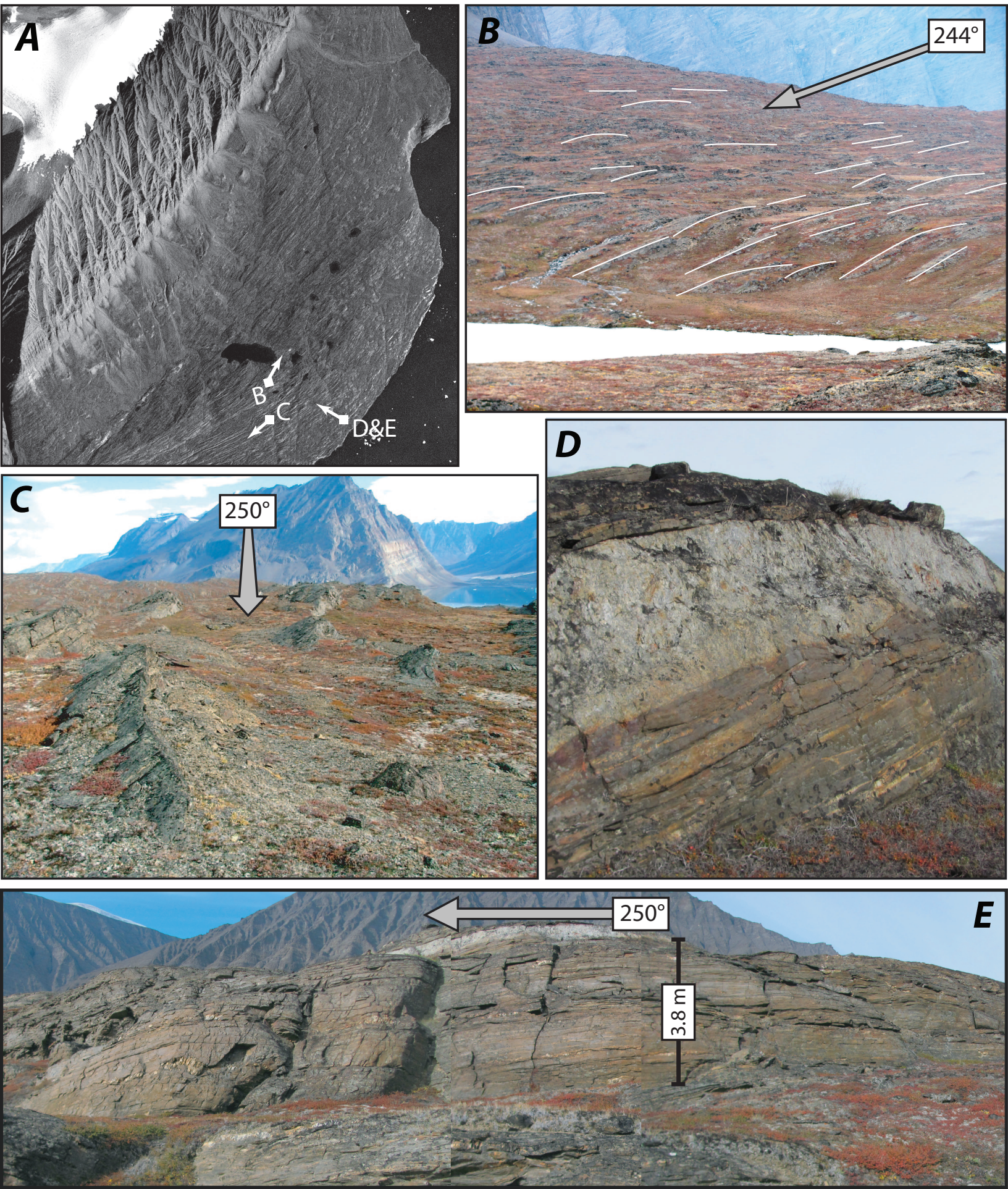

**Figure 6 (Color)**

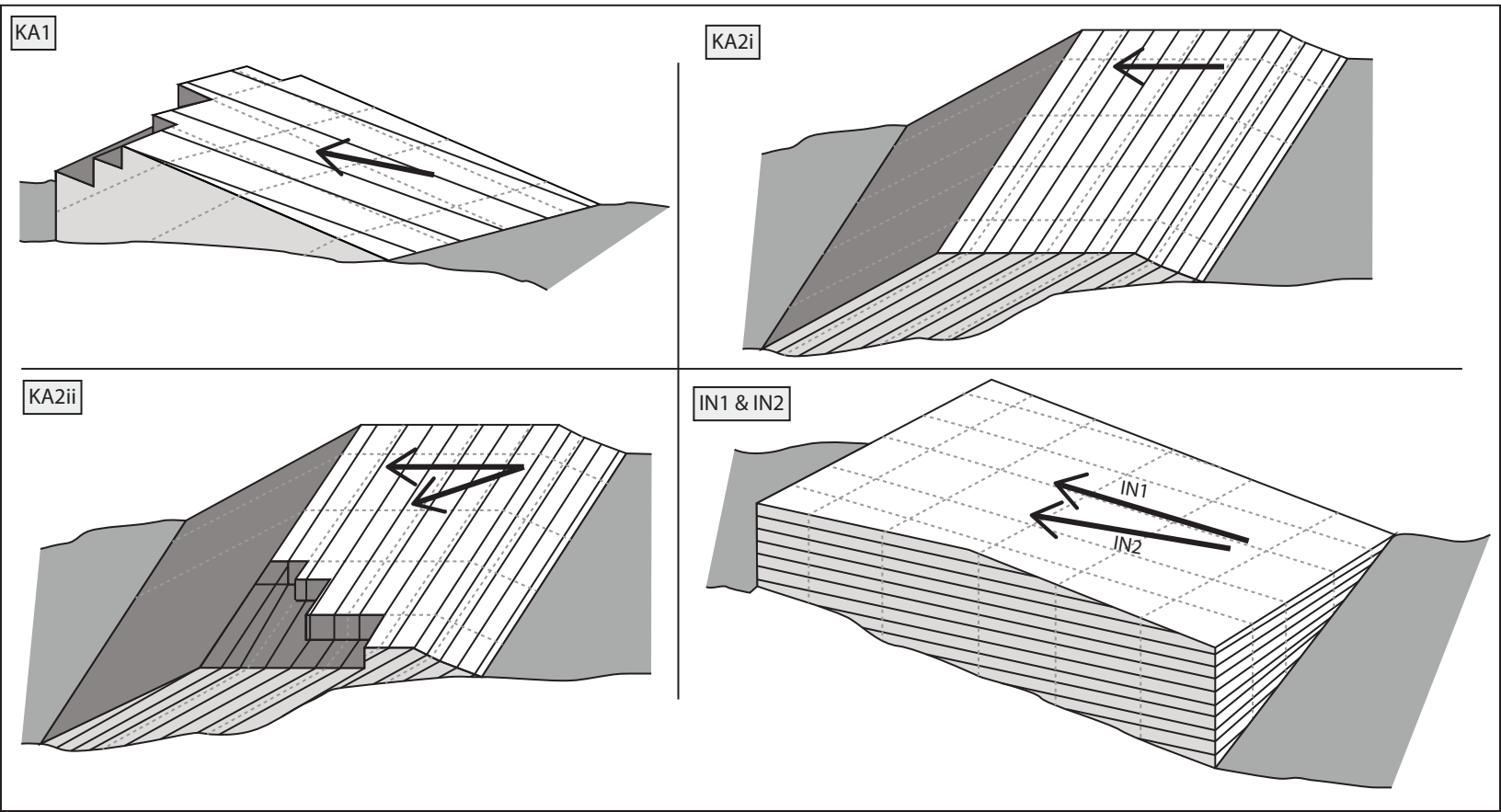

**Figure 7 (Color)**

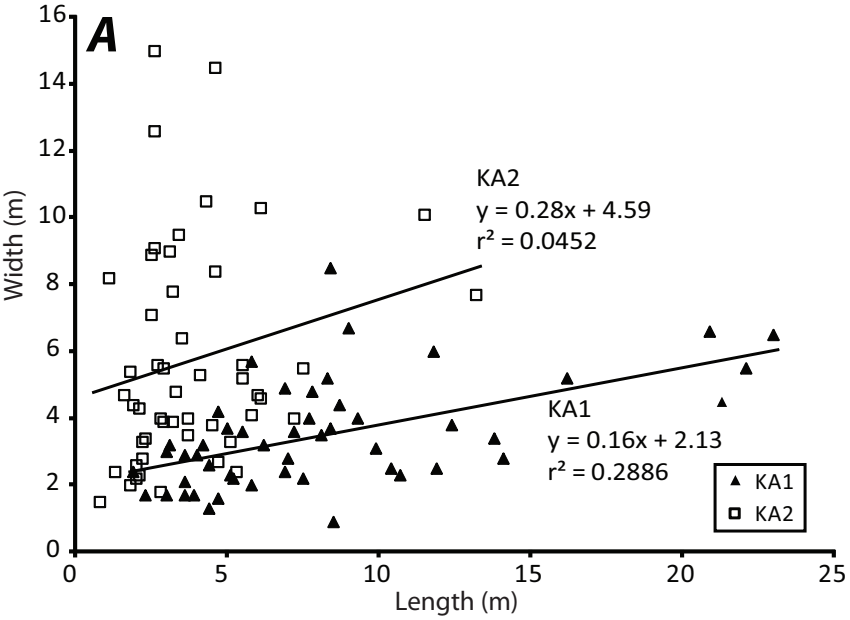


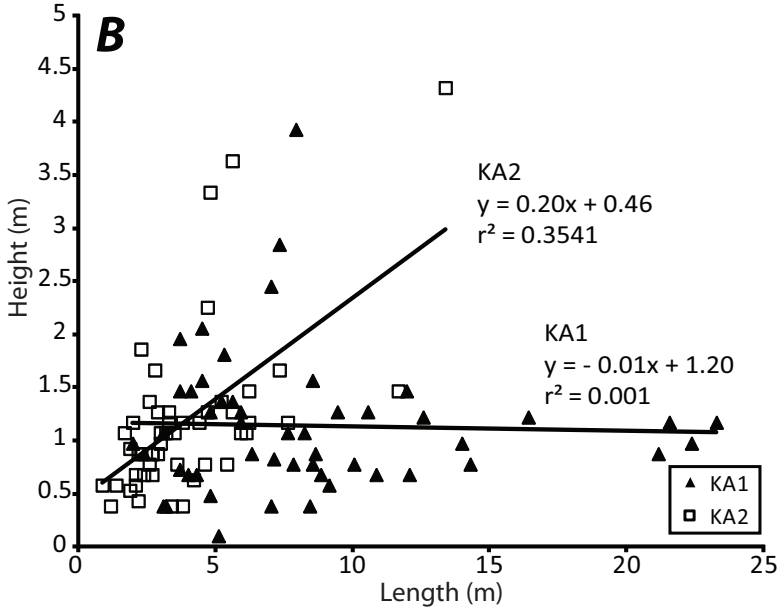


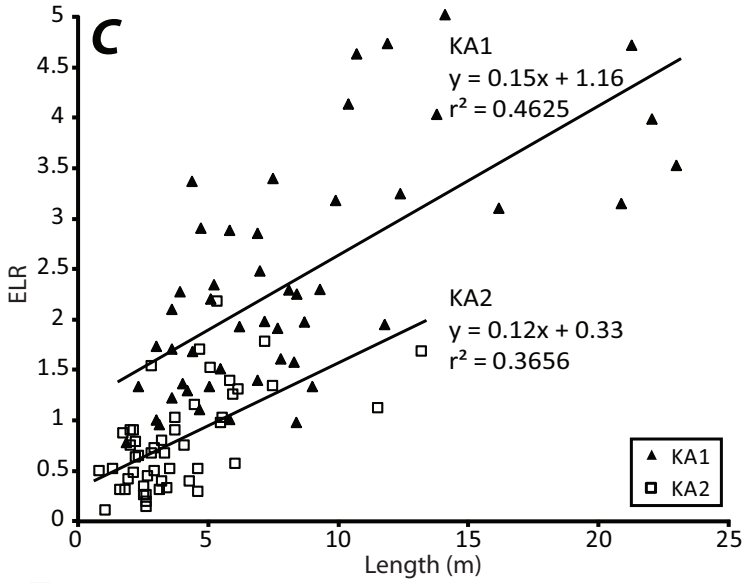


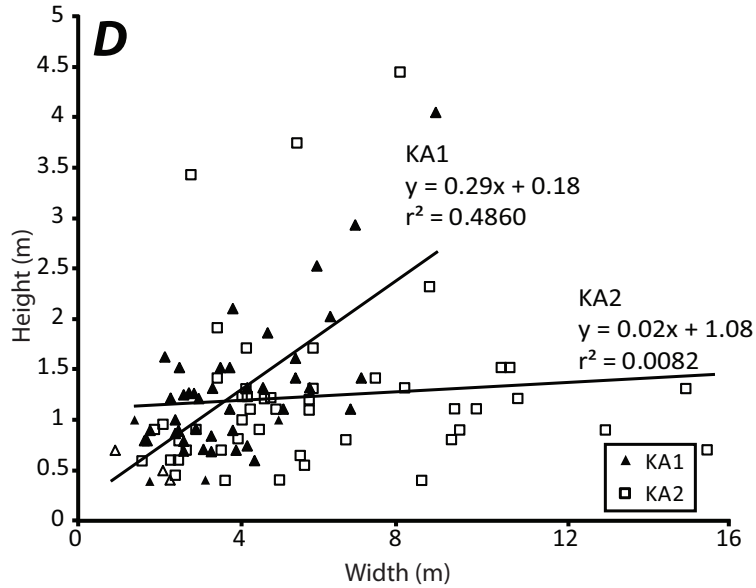


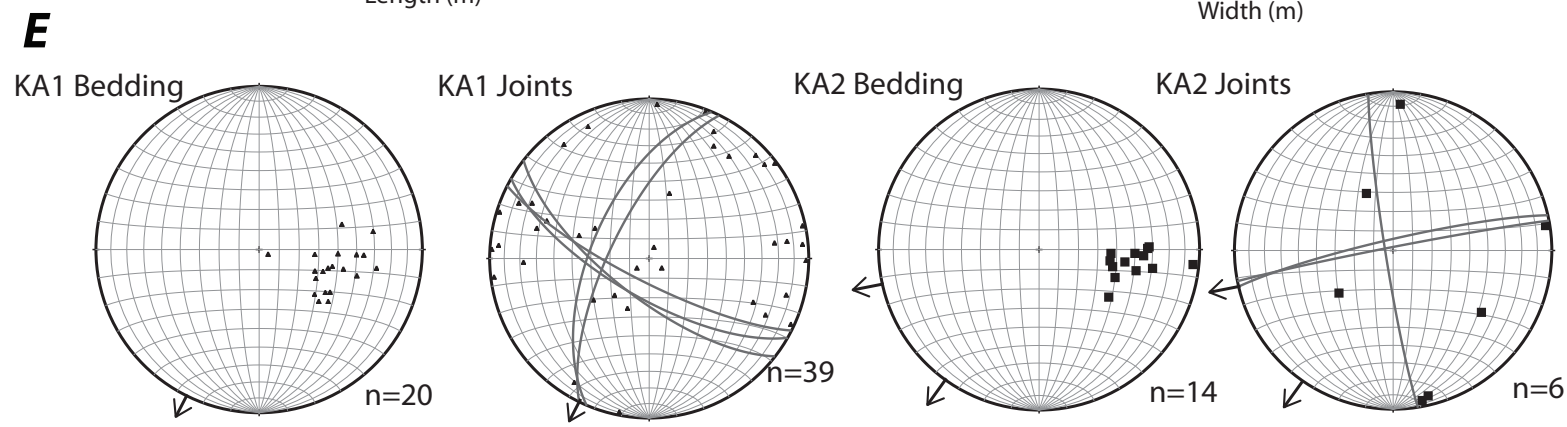

**Figure 8 (Color)**

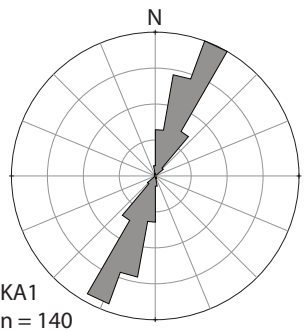


KA1
n = 140
Mean dir. = 201°

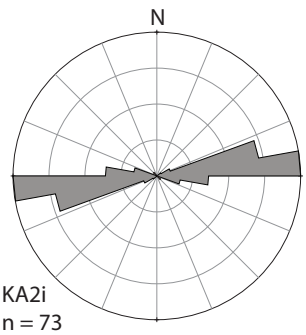


KA2i
n = 73
Mean dir. = 265°

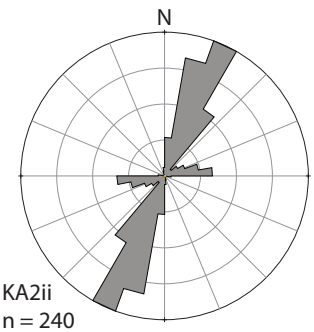


KA2ii
n = 240
Mean dir. = 212°/268°

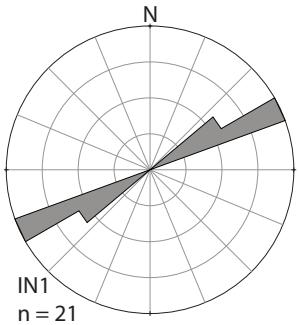


IN1
n = 21
Mean dir. = 243°

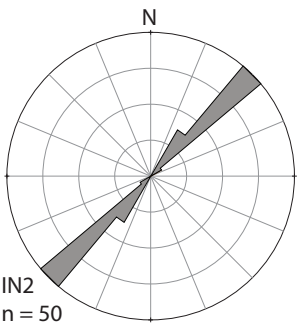


IN2
n = 50
Mean dir. = 225°

**Figure 9 (Color)**

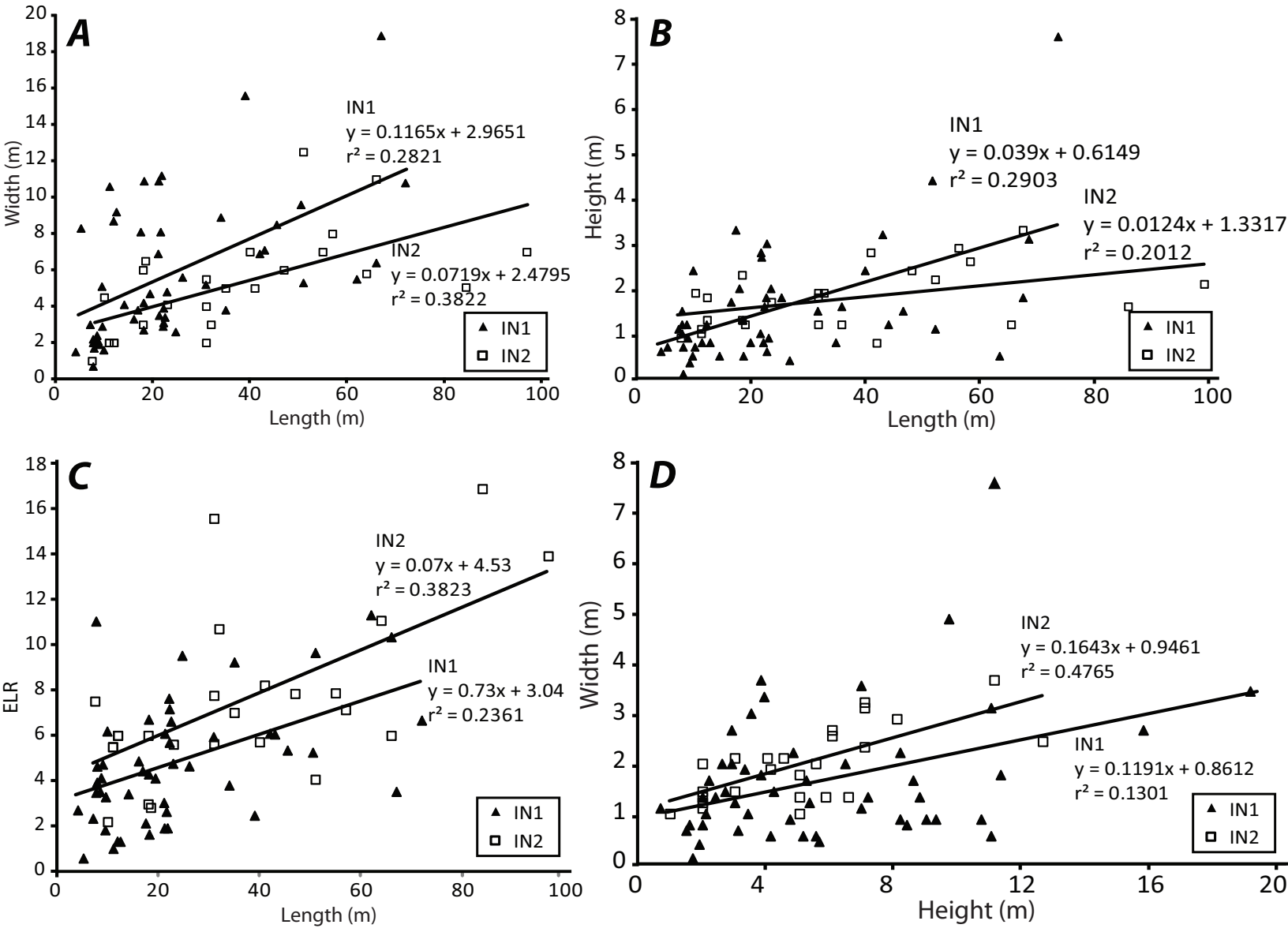


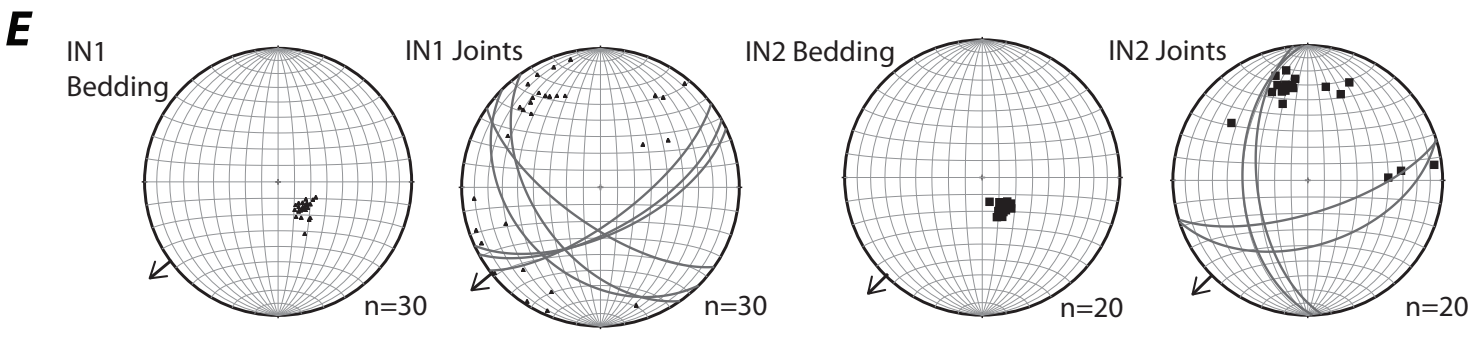

**Figure 10 (Color)**

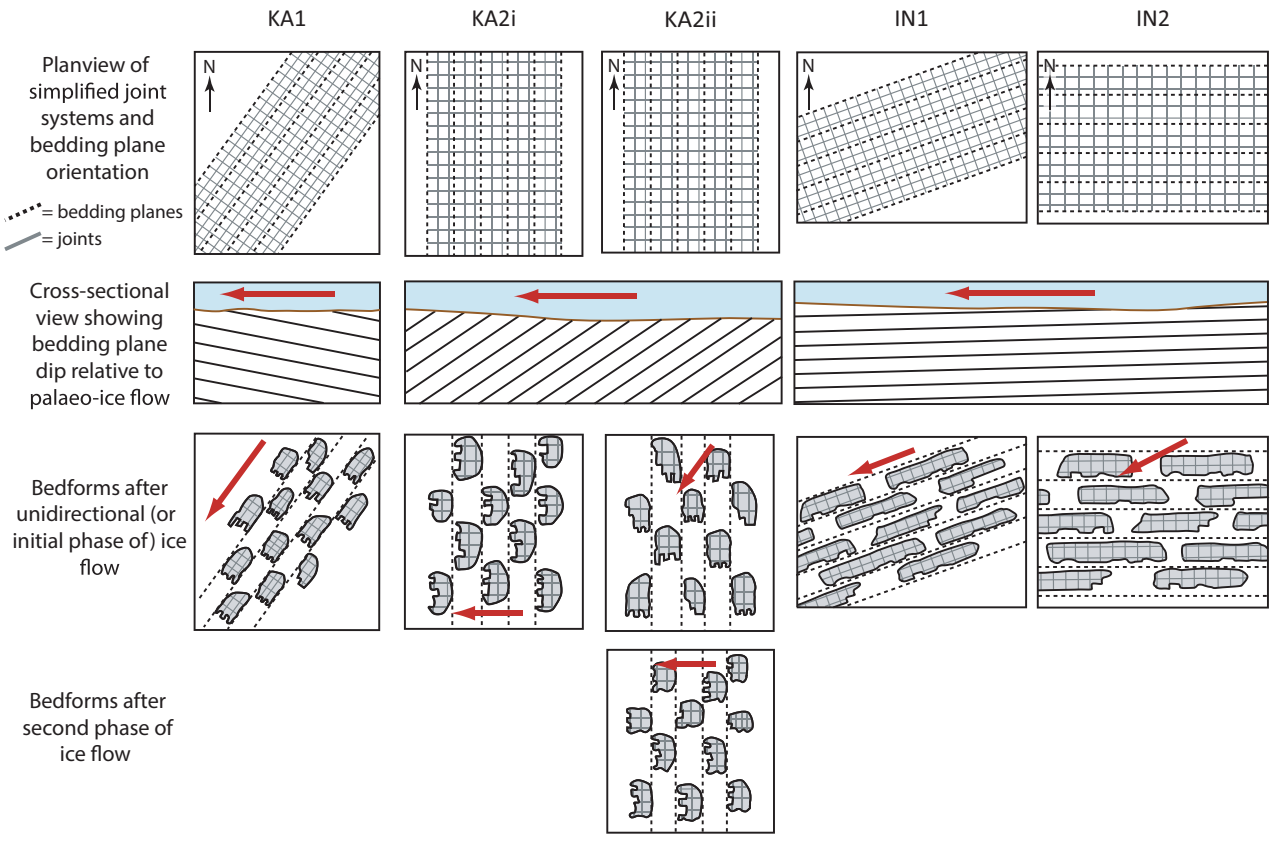

Figure 11 (Color)